Electronic Supplementary Material (ESI) for Organic & Biomolecular Chemistry.

Copper Catalyzed Oxidative Homocoupling of Terminal Alkynes to 1,3-Diynes: $Cu_3(BTC)_2$ MOF as an Efficient and Ligand Free Catalyst for Glaser-Hay Coupling

Supramolecular and Catalysis Lab, Dept. of Natural Products Chemistry,

School of Chemistry, Madurai Kamaraj University, Madurai-625021, India.

*ghemistry@gmail.com, suresh.chem@mkuniversity.org

Table of Contents

1. Characterization of $Cu_3(BTC)_2$ MOF Catalysts:

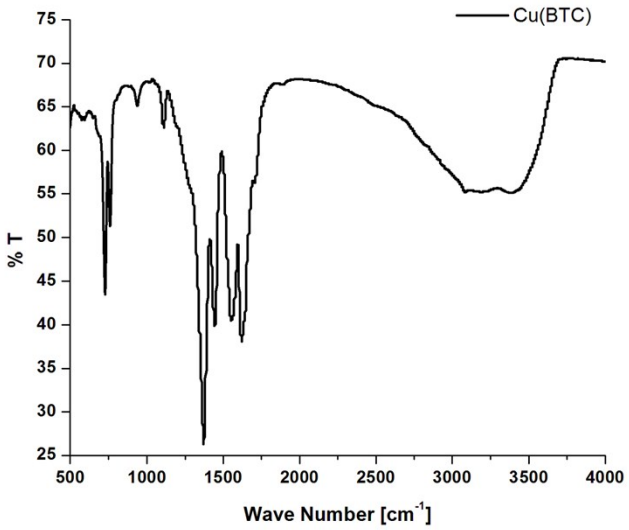

Figure S1. FT-IR spectrum of $Cu_3(BTC)_2$ MOF

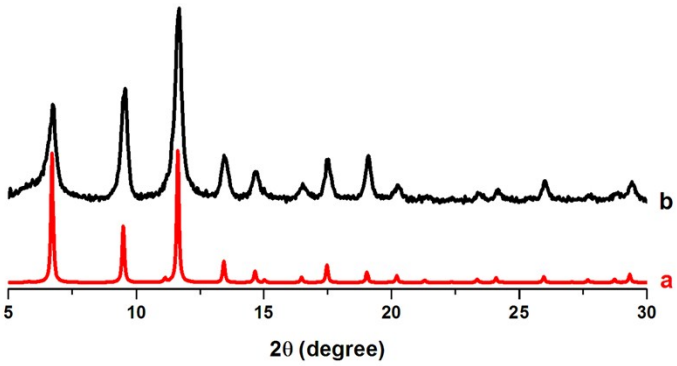

Figure S2 Powder XRD pattern of simulated (a) and as-synthesized $Cu_3(BTC)_2$ MOF (b)

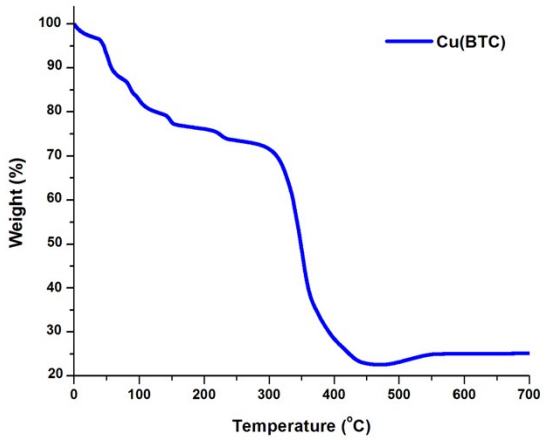

Figure S3 TGA analysis of $Cu_3(BTC)_2$ MOF

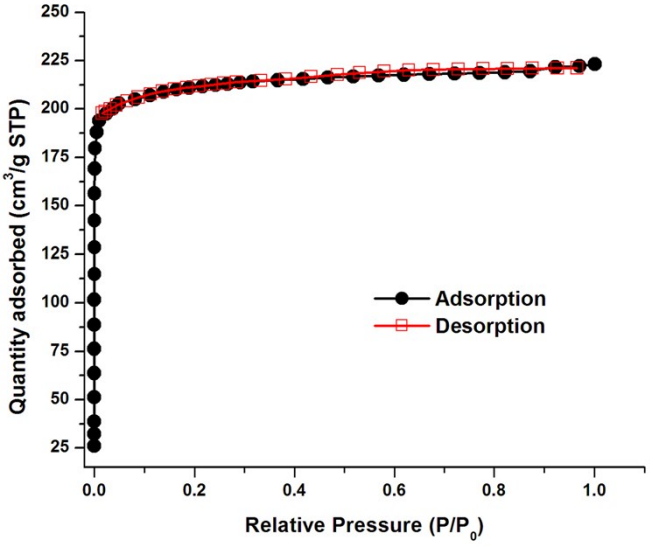

Figure S4 Nitrogen adsorption/desorption isotherm of the $Cu_3(BTC)_2$ MOF

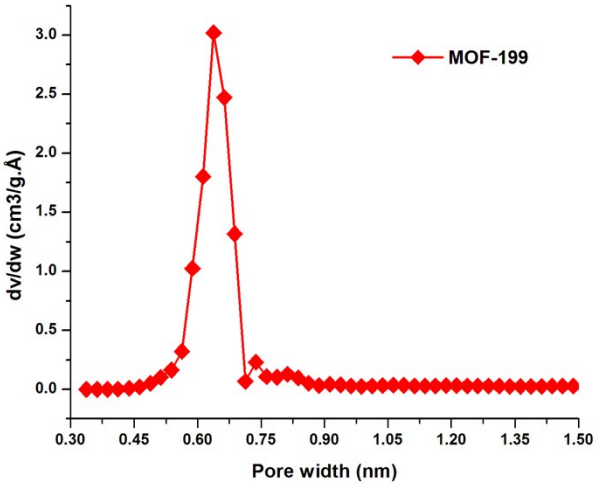

Figure S5 Pore size distribution of the $Cu_3(BTC)_2$ MOF

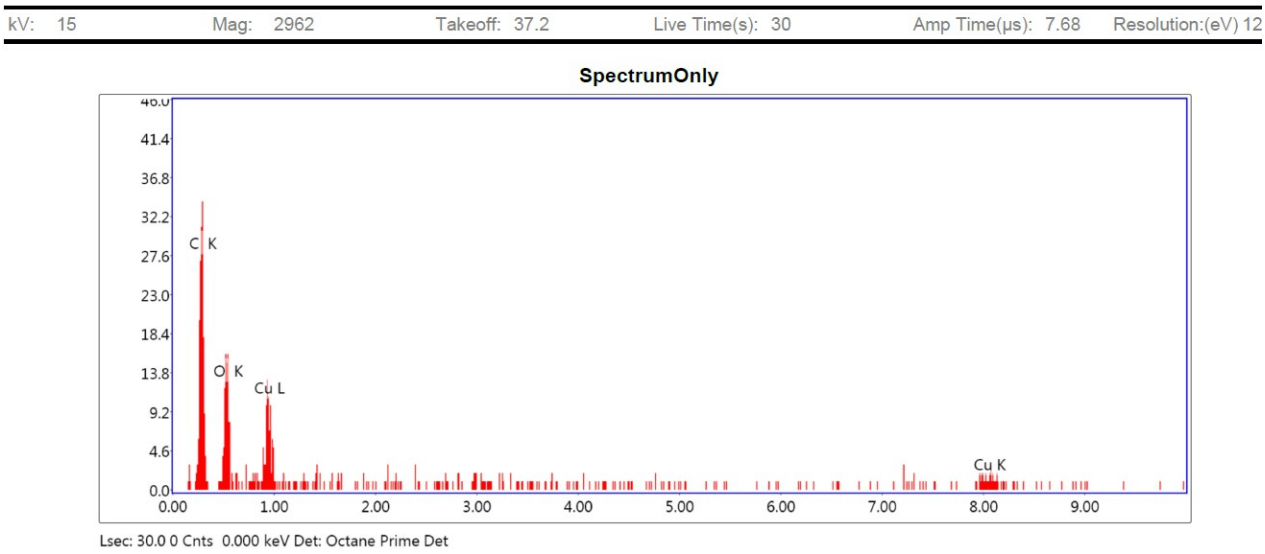

Element	Weight %	Atomic %	Net Int.	Error %	Kratio	Z	R	A	F
C K	48.18	67.18	5.35	15.78	1.0943	0.2208	1.0000	0.9486	0.4188
O K	24.46	25.61	3.14	20.21	1.0435	0.0663	1.0000	0.9702	0.2599
CuK	27.36	7.21	1.21	32.09	0.7406	0.2165	1.0601	1.0491	1.0081

Figure S6 EDAX analysis of $Cu_3(BTC)_2$ MOF

Hot Filtration Test:

To verify, the true heterogeneity of MOF, a control experiment was performed using optimized conditions. The mother liquor was filtered from the reaction mixture after 4 h (66 % of yield) of the reaction by simple filtration. Then the catalyst was again washed with 1 mL of 1,4-dioxane which was the optimized solvent for this reaction. Both the mother liquor and washed solvent was mixed together to get supernatant solution. To this supernatant solution optimized amount of K_2CO_3 was added and allowed to proceed for remaining 8 h without catalyst. Further base was added to the supernatant solution, because the added base was removed during filtration process. After competition of the stipulated time, catalyst removed mother liquor and products conversion was analysed.

1.1 Synthesis and Characterization of $Cu(bpy)(H_2O)_2(BF_4)_2(bpy)$:

$Cu(bpy)(H_2O)_2(BF_4)_2(bpy)$ MOF was synthesized according to the reported literature procedure.[2] First, 4,4'-bipyridine (0.624 g, 2 mmol) in 4 mL of ethanol was slowly added to an 16 mL aqueous solution of $Cu(BF_4)_2 \cdot H_2O$ (0.618 g, 1 mmol) at room temperature and the blue precipitate was formed gradually. The mixture was stirred for 4 h at room temperature, after the solid was filtered off, washed with water and ethanol, dried in air at room temperature and then in vacuum at 100 °C for 2 h and stored under argon. It was characterized using FT-IR, PXRD and elemental analysis. In FT-IR spectrum of $Cu(bpy)(H_2O)_2(BF_4)_2(bpy)$ MOF peaks were present at 3323 and 1301 cm^{-1} due to the bond formation between 4,4'-bipyridine and water molecule in copper salt. Peaks at 1599 and 1666 cm^{-1} were indicated the presence of uncoordinated bipyridine molecules in framework. Elemental analysis by ICP-OES showed the

presence of 6.99 mmolg^{-1} of copper. These characterization results and powder XRD pattern were in good agreement with literature.

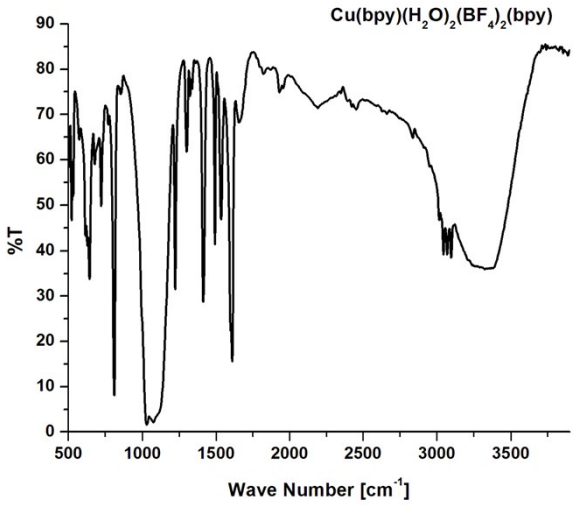

Figure S7 FT-IR spectrum of Cu(bpy)$(H_2O)_2(BF_4)_2$(bpy) MOF

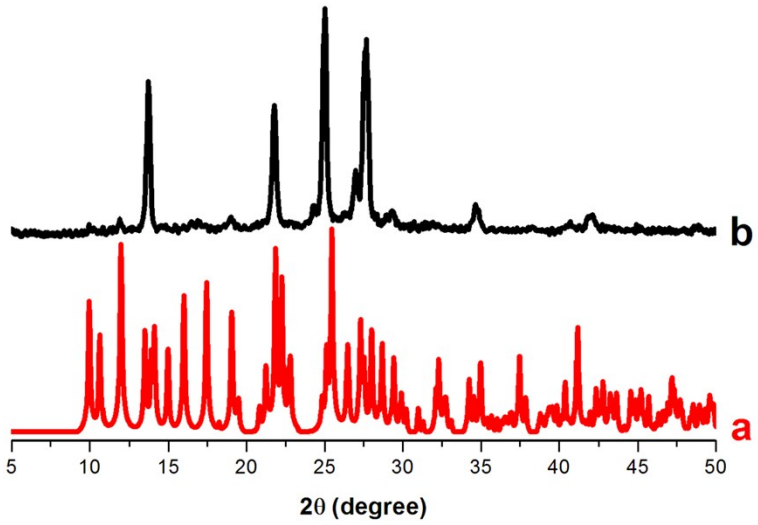

Figure S8 Powder XRD pattern of simulated (a) and as-synthesized Cu(bpy)$(H_2O)_2(BF_4)_2$(bpy) MOF (b)

1.3 Characterization of Cu(tpa) MOF

Cu(tpa) was synthesized by solvothermal process as reported in literature.[3] Copper nitrate trihydrate (8.45 g) and terephthalic acid (5.80 g) was taken in equimolar quantities of 34.9 mmol

in 780 mL of DMF in 1L RB flask, then the mixture was stirred for 30 min. After it was transferred to Teflon lined autoclave and heated in an air-oven up to 110 °C for 36 h. After the reaction was over, the autoclave was cooled slowly to room temperature and small fine blue crystals were found inside the autoclave. Then the mother liquor was simply decanted and washed with DMF to remove unreacted copper nitrate trihydrate and terephthalic acid. The solid was filtered through the Whatman filter paper (No.3). Then repeatedly washed with excess of DMF and dried in a hot air oven at 220 °C for 24 h. In FT-IR spectrum of Cu(tpa) MOF exhibits the peaks at 1666 cm^{-1} indicates that DMF molecule was coordinated to Cu^{II} center and absence of strong absorption bands at 1760–1690 cm^{-1} confirmed the deprotonation of carboxylic acid groups in 1,4-benzene dicarboxylic acid. In Powder XRD, the presence of a very sharp peak nearly at 10.37° indicates that MOF was highly crystalline in nature and the observed pattern exactly matches with reported and simulated patterns. Cu(tpa) MOF was dissolved in dil. HNO_3 and the quantitative analysis by ICP-OES showed 19.93 % of copper was present. These characterization results and powder XRD pattern were in good agreement with literature.

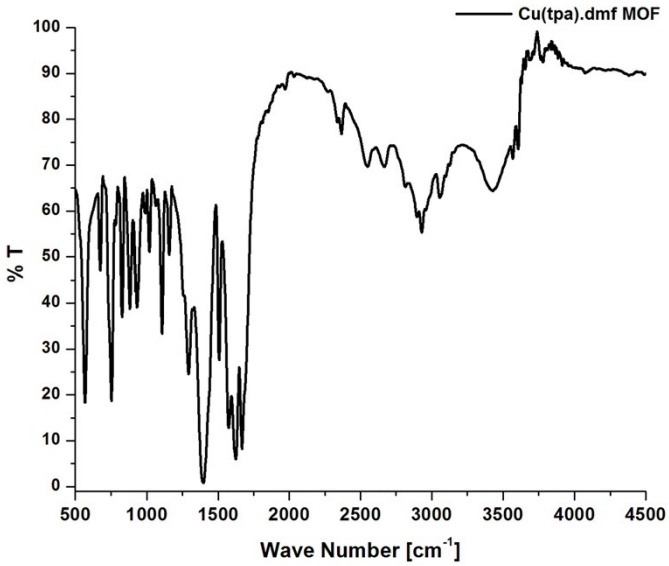

Figure S9 FT-IR spectrum of Cu(tpa) MOF

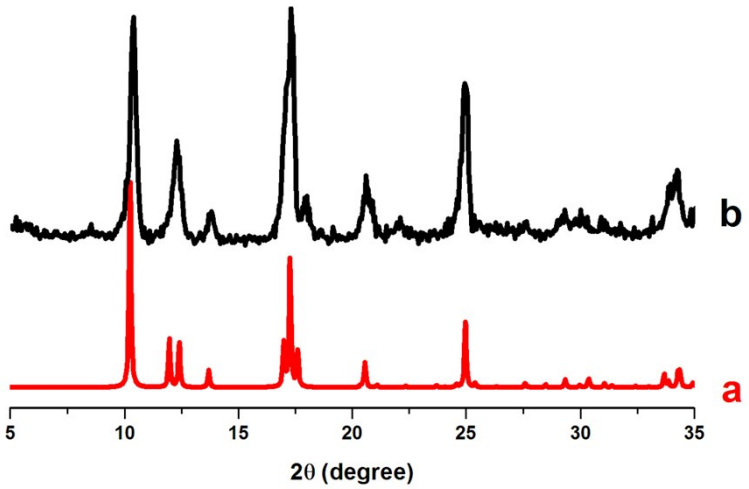

Figure S10 Powder XRD pattern of simulated (a) and as-synthesized Cu(tpa) MOF (b)

1.4 Synthesis of the $Ni_2(BDC)_2(DABCO)$ MOF:

$Ni_2(BDC)_2(DABCO)$ MOF was synthesized according to the reported literature procedure,[4] a solid mixture of H_2BDC (H_2BDC = 1,4 benzenedicarboxylic acid; 2.075 g, 12.49 mmol), DABCO (DABCO = 1,4-diazabicyclo[2.2.2]octane; 0.84 g, 7.49 mmol), and $Ni(NO_3)_2.6H_2O$ (2.9 g, 9.975 mmol) was dissolved in DMF (DMF = N,N'-dimethylformamide; 75 mL). The resulting solution was transferred to Teflon-lined autoclave. Then it was heated at 100 °C in an isothermal oven for 48 h. After cooling the vials to room temperature, the solid product was removed by decanting with mother liquor and washed in DMF (3 x 10 mL) for 3 days. Solvent exchange was carried out with methanol (3 x 10 mL) at room temperature for 3 days. The material was then evacuated under vacuum at 140 °C for 6 h, yielding 0.425 g of $Ni_2(BDC)_2(DABCO)$ in the form of green crystals (72 % yield). In FT-IR spectrum of $Ni_2(BDC)_2(DABCO)$ showed the absence of strong absorption band at 1760–1690 cm^{-1} confirmed the deprotonation of carboxylic acid groups in 1,4-benzene dicarboxylic acid. EDAX analysis of this MOF shows 9.97 wt % of Ni was present. These characterization results and powder XRD pattern were in good agreement with literature.

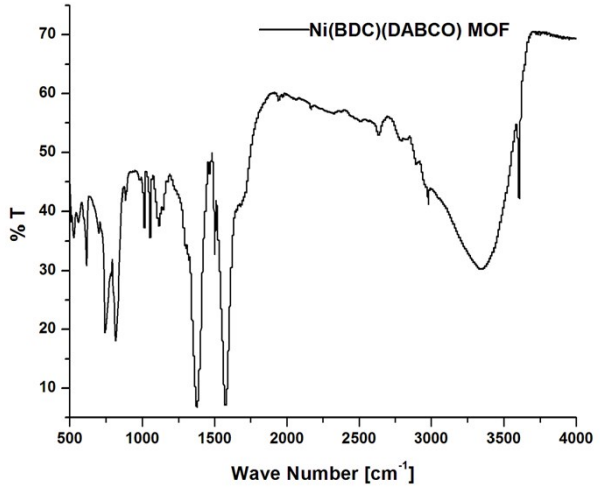

Figure S11 FT-IR spectrum of $Ni_2(BDC)_2(DABCO)$ MOF

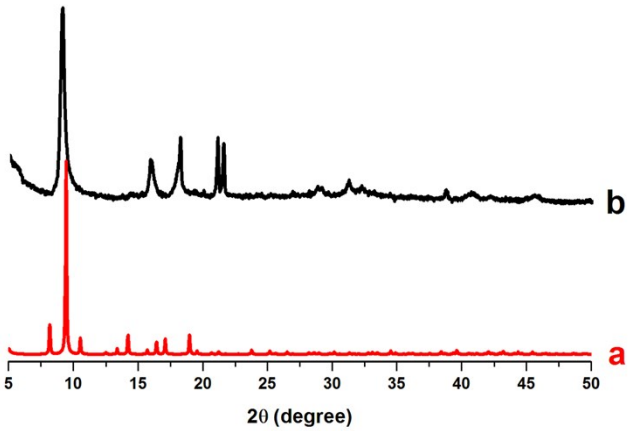

Figure S12 Powder XRD pattern of simulated (a) and as-synthesized $Ni_2(BDC)_2(DABCO)$ MOF (b)

1.5 Synthesis and Characterization of Fe(BTC) MOF:

Fe(BTC) MOF was prepared according to the reported literature.[5] The reactants $Fe(NO_3)_3 \cdot 9H_2O$ (2.5 mmol) and 1,3,5-benzenetricarboxylicacid (H_3BTC, 3.1 mmol) with a 1:1 molar ratio were dissolved in 40 mL of DMF. The mixture was heated at 150 °C for 24 h in a Teflon lined stainless steel autoclave. After cooled to room temperature, the solid was filtered off and washed with DMF and ethanol for several times, then dried at 60 °C in vacuum for 6 h. The dried Fe(BTC) MOF powder was obtained and characterized. In FT-IR, the absence of strong

absorption bands at 1760–1690 cm^{-1} and the presence of strong peak at 1620 cm^{-1} were due to the deprotonation of –COOH groups in benzene tricarboxylic acid, which is lower than the C=O stretching vibrations of carboxylic acids and confirmed the formation of Fe(BTC) MOF. Elemental analysis by ICP-OES showed the iron loading was 2.675 $mmolg^{-1}$. Observed results and PXRD pattern were good agreement reported values.

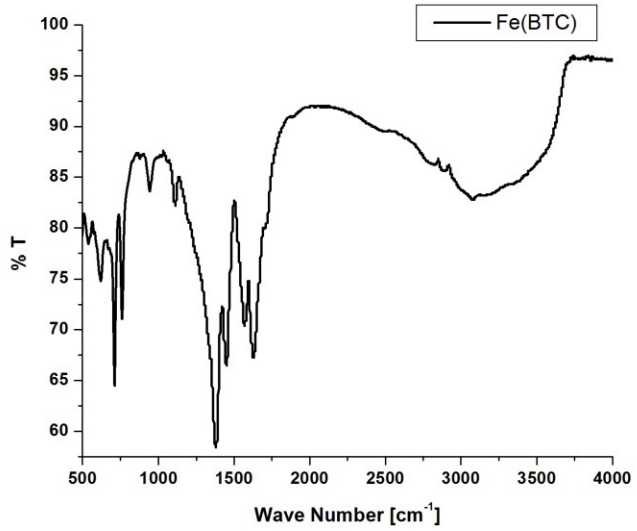

Figure S13 FT-IR spectrum of Fe(BTC) MOF

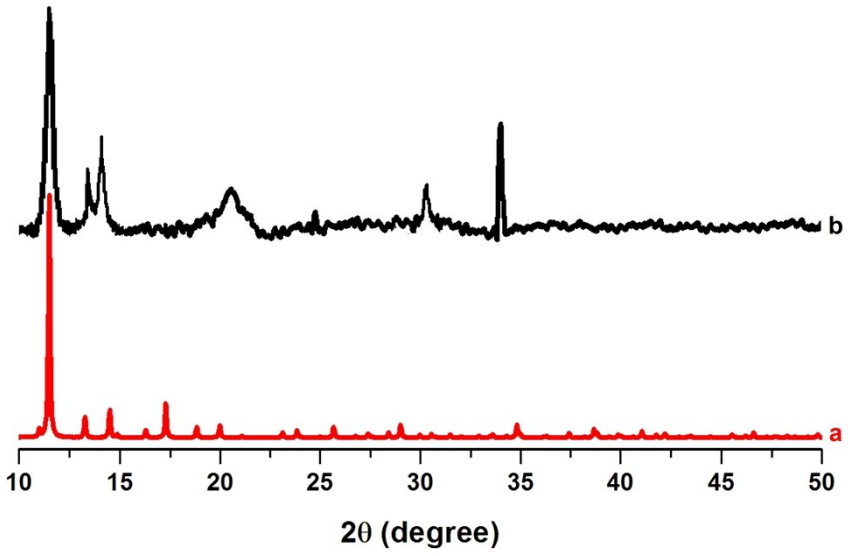

Figure S14 Powder XRD pattern of simulated (a) and as-synthesized Fe(BTC) MOF (b)

1.6 Synthesis and Characterization of Fe-MIL-53:

Fe-MIL-53 was prepared according to the reported literature.[6] 4.04 g (10 mmol) of terephthalic acid, 1.66 g (10 mmol) of iron(III) nitrate nonahydrate and 100 mL of DMF were placed in a stainless steel autoclave and heated for 48 h. Crude MIL-53(Fe)-$(H_2\text{-BDC})_x$ was recovered as an orange solid by filtration, washed with DMF, acetone and dried in air. Then the solid was dried at 100 °C under vacuum for 8 h. The PXRD pattern and FT-IR analysis were good agreement with reported. The absence of strong absorption bands at 1760–1690 cm^{-1} was due to the deprotonation of –COOH groups in benzene dicarboxylic acid and the presence of strong peak at 1625 cm^{-1}, which was lower than the C=O stretching vibrations of carboxylic acids revealed the formation of Fe-MIL-53 MOF.

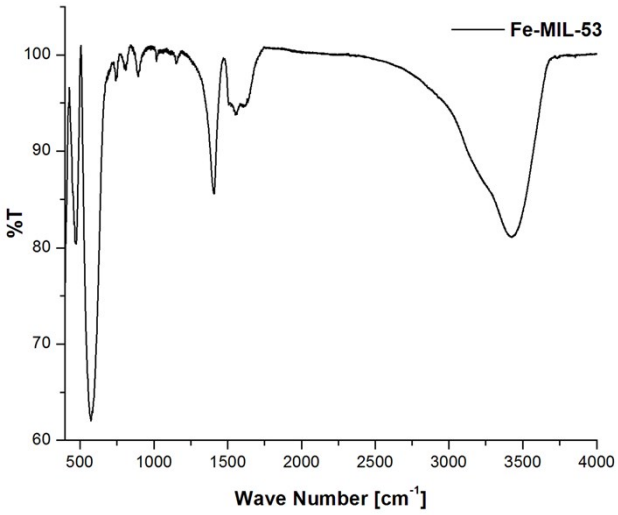

Figure S15 FT-IR spectrum of Fe-MIL-53 MOF

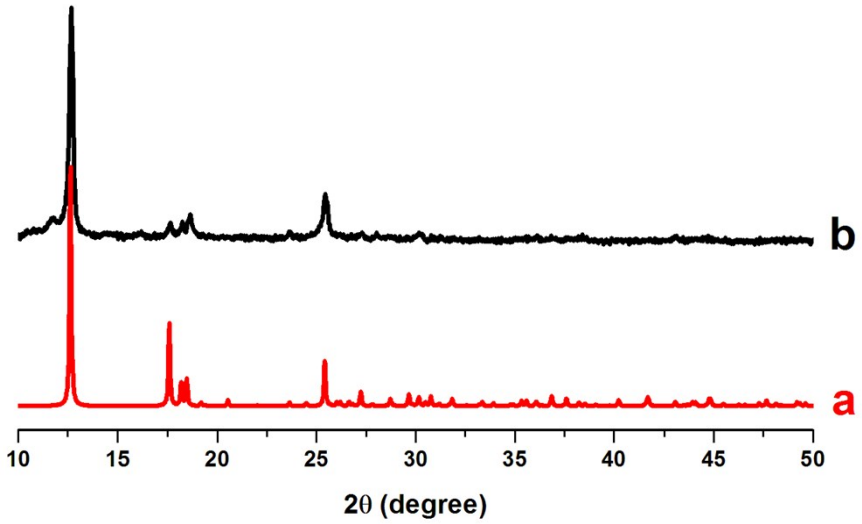

Figure S16 Powder XRD pattern of simulated (a) and as-synthesized Fe-MIL-53 MOF (b)

1.7 Synthesis and Characterization of IRMOF-3:

IRMOF-3 was prepared by solvothermal process as reported in literature.[7] $Zn(NO_3)_2.6H_2O$ (21 g, 70.6 mmol) and 2-aminoterephthalic acid (5.25 g, 28.9 mmol) were dissolved in 700 mL of DMF. The mixture was stirred for 30 minutes. Then it was transferred to a Teflon lined autoclave and heated in an air-oven up to 100 °C for 18 h. After, the autoclave was cooled to room temperature and then brownish color crystals were filtered off and washed with excess of DMF to remove unreacted reactants. Resulted crystals were immersed in 40 mL of $CHCl_3$ for three days by changing fresh $CHCl_3$ every day. After, the soaked crystals were stored in the $CHCl_3$ until further use. In FT-IR spectrum, the absence of strong absorption bands at 1760–1690 cm^{-1} and the strong peak at 1566 cm^{-1}, which was lower than the C=O stretching vibrations of carboxylic acids were confirmed the deprotonation of carboxylic acid group of 2-aminoterephthalic acid. Peak at 3290 cm^{-1} showed the presence of free amine group in IRMOF-3. Observed results and PXRD pattern were in good agreement with those reported.

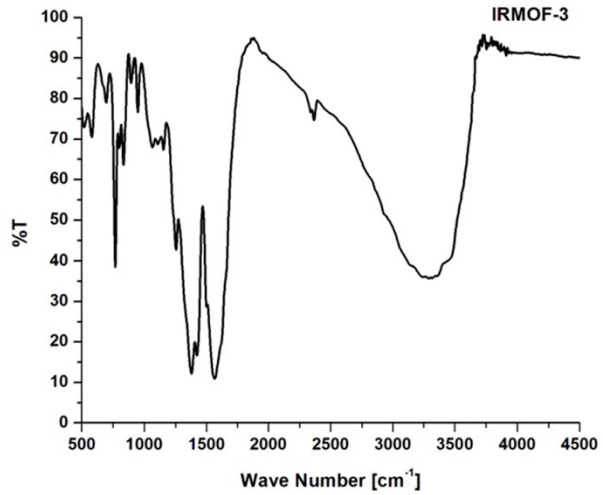

Figure S17 FT-IR spectrum of IRMOF-3

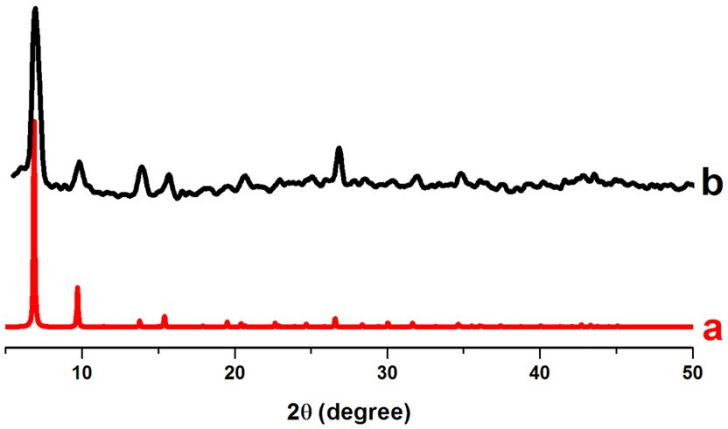

Figure S18 Powder XRD pattern of simulated (a) and as-synthesized IRMOF-3 (b)

2. NMR and EI-MS data:

1,4-diphenylbuta-1,3-diyne (3a) ^{1}H NMR (300 MHz, $CDCl_3$) δ: 7.38–7.32 (m, 6H), 7.56–7.51 (m, 4H). **(Fig. S19)** ^{13}C NMR (75 MHz, $CDCl_3$) δ: 73.98, 81.59, 121.89, 128.42, 129.17, 132.50. **(Fig. S20)** EI-MS: 202 **(Fig. S51)**	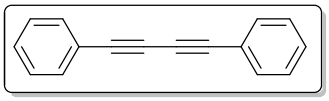
1,4-di-*p*-tolylbuta-1,3-diyne (3b) ^{1}H NMR (300 MHz, $CDCl_3$) δ: 2.36 (s, 6H), 7.14 (d, 4H, *J* = 8.2 Hz), 7.41 (d, 4H, *J* = 8.1 Hz). **(Fig. S21)** ^{13}C NMR (75 MHz, $CDCl_3$) δ: 21.60, 73.42, 81.52, 118.75, 129.18, 132.36, 139.46. **(Fig. S22)** EI-MS: 230 **(Fig. S52)**	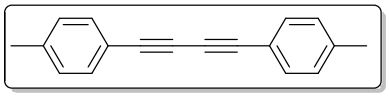
1,4-bis(4-ethylphenyl)buta-1,3-diyne (3c) ^{1}H NMR (300 MHz, $CDCl_3$) δ: 1.23 (t, 6H, *J* = 7.6 Hz), 2.66 (q, 4H, *J* = 7.6 Hz), 7.17 (d, 4H, *J* = 8.0 Hz), 7.45 (d, 4H, *J* = 8.1 Hz). **(Fig. S23)** ^{13}C NMR (75 MHz, $CDCl_3$) δ: 15.14, 28.82, 73.50, 81.52, 118.91, 127.92, 132.37, 145.60. **(Fig. S24)** EI-MS: 258 **(Fig. S53)**	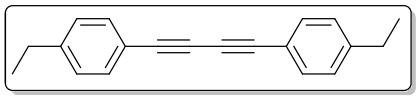
1,4-bis(4-(tert-butyl)phenyl)buta-1,3-diyne (3d) ^{1}H NMR (300 MHz, $CDCl_3$) δ: 1.32 (s, 18H), 7.36 (d, 4H, *J* = 8.6 Hz), 7.47 (d, 4H, *J* = 8.6 Hz). **(Fig. S25)** ^{13}C NMR (75 MHz, $CDCl_3$) δ: 31.08, 34.85, 73.55, 81.50, 118.85, 125.43, 132.25, 152.52. **(Fig. S26)** EI-MS: 315 **(Fig. S54)**	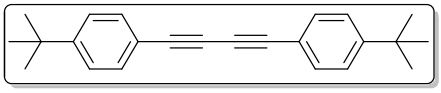
1,4-bis(4-methoxyphenyl)buta-1,3-diyne (3e) ^{1}H NMR (300 MHz, $CDCl_3$) δ: 3.82 (s, 6H), 6.85 (d, 4H, *J* = 8.7 Hz), 7.46 (d, 4H, *J* = 8.8 Hz). **(Fig. S27)** ^{13}C NMR (75 MHz, $CDCl_3$) δ: 55.31, 72.92, 81.21, 113.89, 114.10, 134.01, 160.20. **(Fig. S28)**	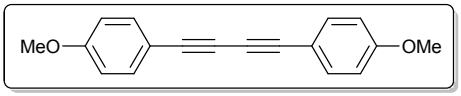

EI-MS: 262 **(Fig. S55)**	
<u>1,4-bis(2-methoxyphenyl)buta-1,3-diyne (3f)</u> ^{1}H NMR (300 MHz, $CDCl_3$) δ: 3.83 (s, 6H), 6.82 (dd, 2H, *J* = 3.7, 4.7 Hz), 6.86 (dd, 2H, *J* = 0.9, 7.5 Hz), 7.25 (ddd, 2H, *J* = 1.7, 7.6, 8.3 Hz), 7.41 (dd, 2H, *J* = 1.7, 7.6 Hz). **(Fig. S29)** ^{13}C NMR (75 MHz, $CDCl_3$) δ: 55.62, 77.84, 78.60, 110.54, 110.99, 120.34, 130.48, 134.16, 161.17. **(Fig. S30)** EI-MS: 262 **(Fig. S56)**	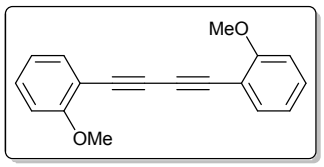
<u>1,4-bis(4-propoxyphenyl)buta-1,3-diyne (3g)</u> ^{1}H NMR (300 MHz, $CDCl_3$) δ: 0.96 (t, 6H, *J* = 7.4 Hz), 1.67–1.81 (m, 4H), 3.85 (t, 4H, *J* = 6.6 Hz), 6.77 (t, 4H, *J* = 5.6 Hz), 7.33–7.41(m, 4H). **(Fig. S31)** ^{13}C NMR (75 MHz, $CDCl_3$) δ: 9.47, 21.48, 68.56, 71.90, 80.31, 112.64, 113.61, 132.99, 158.81. **(Fig. S32)**	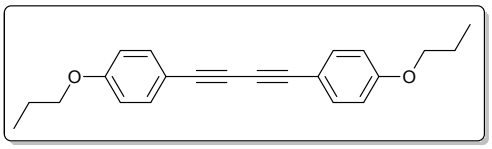
<u>1,4-bis(4-(benzyloxy)phenyl)buta-1,3-diyne (3h)</u> ^{1}H NMR (300 MHz, $CDCl_3$) δ: 5.08 (s, 4H), 6.93 (d, 4H, *J* = 8.7 Hz), 7.40 (m, 14H). **(Fig. S33)** ^{13}C NMR (75 MHz, $CDCl_3$) δ: 70.04, 73.00, 81.19, 114.17, 114.99, 127.45, 128.14, 128.64, 134.04, 136.37, 159.37. **(Fig. S34)** EI-MS: 234 **(Fig. S57)**	
<u>1,4-bis(4-fluorophenyl)buta-1,3-diyne (3i)</u> ^{1}H NMR (300 MHz, $CDCl_3$) δ: 7.00–7.08 (m, 4H), 7.48–7.55 (m, 4H). **(Fig. S35)** ^{13}C NMR (75 MHz, $CDCl_3$) δ: 164.78, 161.45, 134.59, 134.48, 117.94, 117.90, 116.05, 115.75, 80.45, 73.61. **(Fig. S36)** EI-MS: 238 **(Fig. S58)**	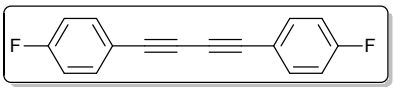

1,4-bis(3-fluorophenyl)buta-1,3-diyne (3j) ^{1}H NMR (300 MHz, $CDCl_3$) δ: 7.10 (ddd, 2H, *J* = 3.1, 5.8, 11.8 Hz), 7.19–7.25 (m, 2H), 7.32 (ddd, 4H, *J* = 1.7, 3.4, 4.3 Hz). **(Fig. S37)** ^{13}C NMR (75 MHz, $CDCl_3$) δ: 74.39, 80.59, 116.77, 117.05, 119.07, 119.37, 123.29, 123.41, 128.44, 128.49, 130.08, 130.19, 160.61, 163.89. **(Fig. S38)** EI-MS: 238 **(Fig. S59)**	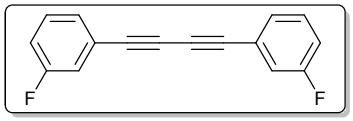
1,4-bis(3-chlorophenyl)buta-1,3-diyne (3k) ^{1}H NMR (300 MHz, $CDCl_3$) δ: 7.26–7.32(m, 2H), 7.34–7.39 (m, 2H), 7.41 (dt, 2H, *J* = 1.3, 7.5 Hz), 7.51 (t, 2H, *J* = 1.7 Hz). **(Fig. S39)** ^{13}C NMR (75 MHz, $CDCl_3$) δ: 74.67, 80.54, 123.26, 129.70, 130.64, 132.25, 134.34. **(Fig. S40)** EI-MS: 270, 272, 271**(Fig. S60)**	
3,3'-(buta-1,3-diyne-1,4-diyl)dianiline (3l) ^{1}H NMR (300 MHz, $CDCl_3$) δ: 3.55–3.77 (m, 4H), 6.61 (dt, 2H, *J* = 11.1, 17.8 Hz), 6.77 (d, 2H, *J* = 13.4 Hz), 6.82–6.89 (m, 2H), 7.04 (t, 2H, *J* = 7.8 Hz). **(Fig. S41)** ^{13}C NMR (75 MHz, $CDCl_3$) δ: 73.33, 81.62, 116.21, 118.31, 122.33, 122.83, 129.30, 146.26. **(Fig. S42)** EI-MS: 232 **(Fig. S61)**	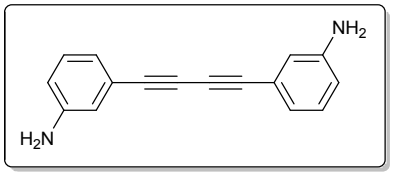
1,4-di(cyclohex-1-en-1-yl)buta-1,3-diyne (3m) ^{1}H NMR (300 MHz, $CDCl_3$) δ: 1.60 (d, 8H, *J* = 4.1 Hz), 2.12 (d, 8H, *J* = 3.8 Hz), 6.25 (s, 2H). **(Fig. S43)** ^{13}C NMR (75 MHz, $CDCl_3$) δ: 21.27, 22.09, 25.83, 28.65, 71.52, 82.64, 119.90, 138.05. **(Fig. S44)** EI-MS: 210 **(Fig. S62)**	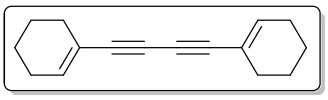
1,1'-(buta-1,3-diyne-1,4-diyl)dicyclohexanol (3n) ^{1}H NMR (300 MHz, $CDCl_3$) δ: 1.51–1.74 (m, 12 H),	

1.94 (dd, 8 H, J = 14.9, 28.9 Hz). **(Fig. S45)** ^{13}C NMR (75 MHz, $CDCl_3$) δ: 22.82, 24.84, 39.40, 67.84, 68.20, 83.32. **(Fig. S46)** EI-MS: **(Fig. S63)**	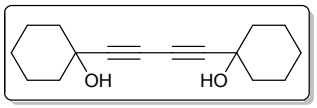
2,2,7,7-tetramethylocta-3,5-diyne (3o) ^{1}H NMR (300 MHz, $CDCl_3$) δ: 1.24 (s, 18H). **(Fig. S47)** ^{13}C NMR (75 MHz, $CDCl_3$) δ: 27.90, 30.58, 63.74, 86.07. **(Fig. S48)** EI-MS: 162 **(Fig. S64)**	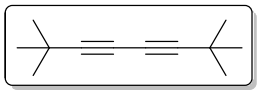
Hexa-2,4-diyne-1,6-diol (3p) ^{1}H NMR (300 MHz, $CDCl_3$) δ: 4.36 (s, 4H). **(Fig. S49)** ^{13}C NMR (75 MHz, $CDCl_3$) δ: 50.41, 68.79, 78.11. **(Fig. S50)** EI-MS: 110 **(Fig. S65)**	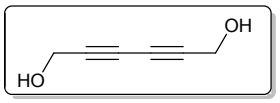

3. References:

1. (a) S. S. -Y. Chui, S. M. -F. Lo, J. P. H. Charmant, A. G. Orpen and I. D. Williams, *Science,* 1999, **283,** 1148; (b) D. J. Tranchemontagne, J. R. Hunt and O. M. Yaghi, *Tetrahedron,* 2008, **64,** 8553; (c) L. T. L. Nguyen, T. T. Nguyen, K. D. Nguyen and N. T. S. Phan, *Appl. Catal., A: Gen.* 2012, **425,** 44.
2. D. Jiang, T. Mallat, F. Krumeich and A. Baiker, *J. Catal.,* 2008, **257,** 390.
3. C. G. Carson, K. Hardcastle, J. Schwartz, X. Liu, C. Hoffmann, R. A. Gerhardt and R. Tannenbaum, *Eur. J. Inorg. Chem.,* 2009, 2338.
4. T. Truong, C. K. Nguyen, T. V. Tran, T. T. Nguyen and N. T. S. Phan, *Catal. Sci. Technol.,* 2014, **4,** 1276.
5. B. -J. Zhu, X. -Y. Yu, Y. Jia, F. -M. Peng, B. Sun, M. -Y. Zhang, T. Luo, J. -H. Liu, X. -J. Huang, *J. Phys. Chem. C.* 2012, **116,** 8601.
6. P. Horcajada, C. Serre, G. Maurin, N. A. Ramsahye, F. Balas, M. V. -Regi, M. Sebban, F. Taulelle and G. Ferey, *J. Am. Chem. Soc.,* 2008, **130,** 6774.
7. F. X. L. Xamena, F. G. Cirujano and A. Corma, *Microporous Mesoporous Mater.,* 2012, **157,** 112.

4. NMR Spectra of isolated Compounds from 3a – 3p:

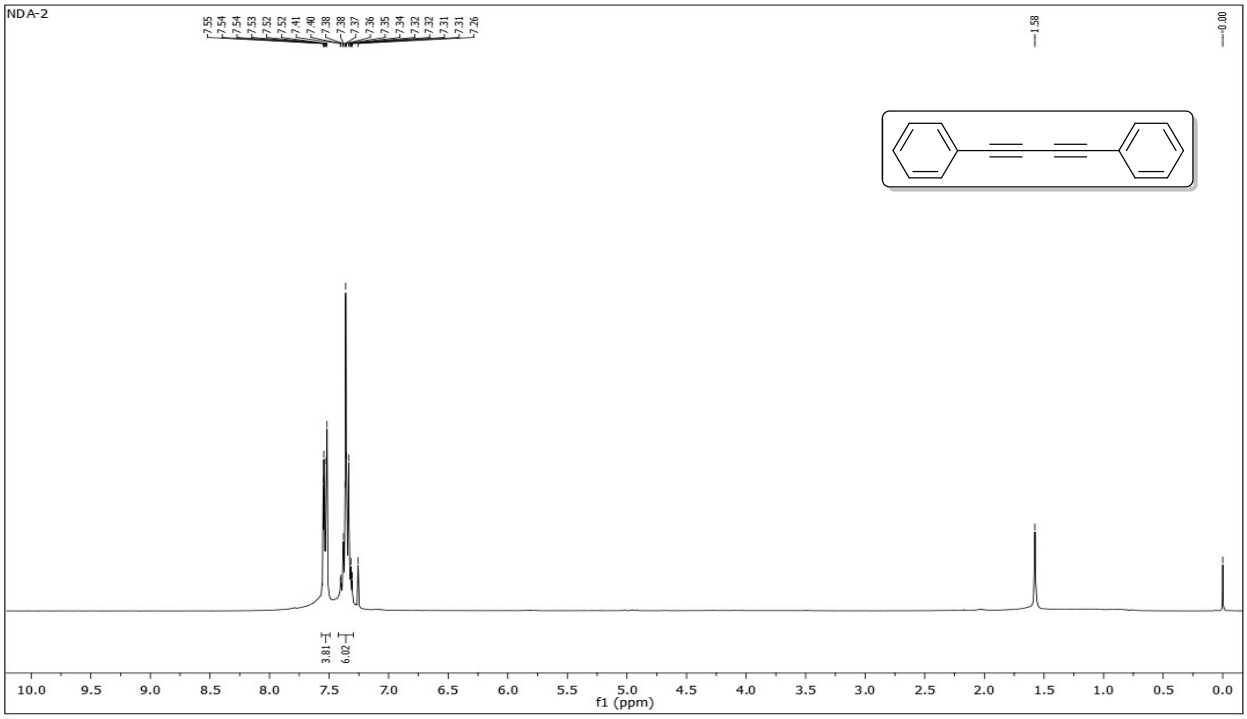

Fig. S19 ^{1}H NMR spectrum of 1,4-diphenylbuta-1,3-diyne **3a** (300 MHz, $CDCl_3$)

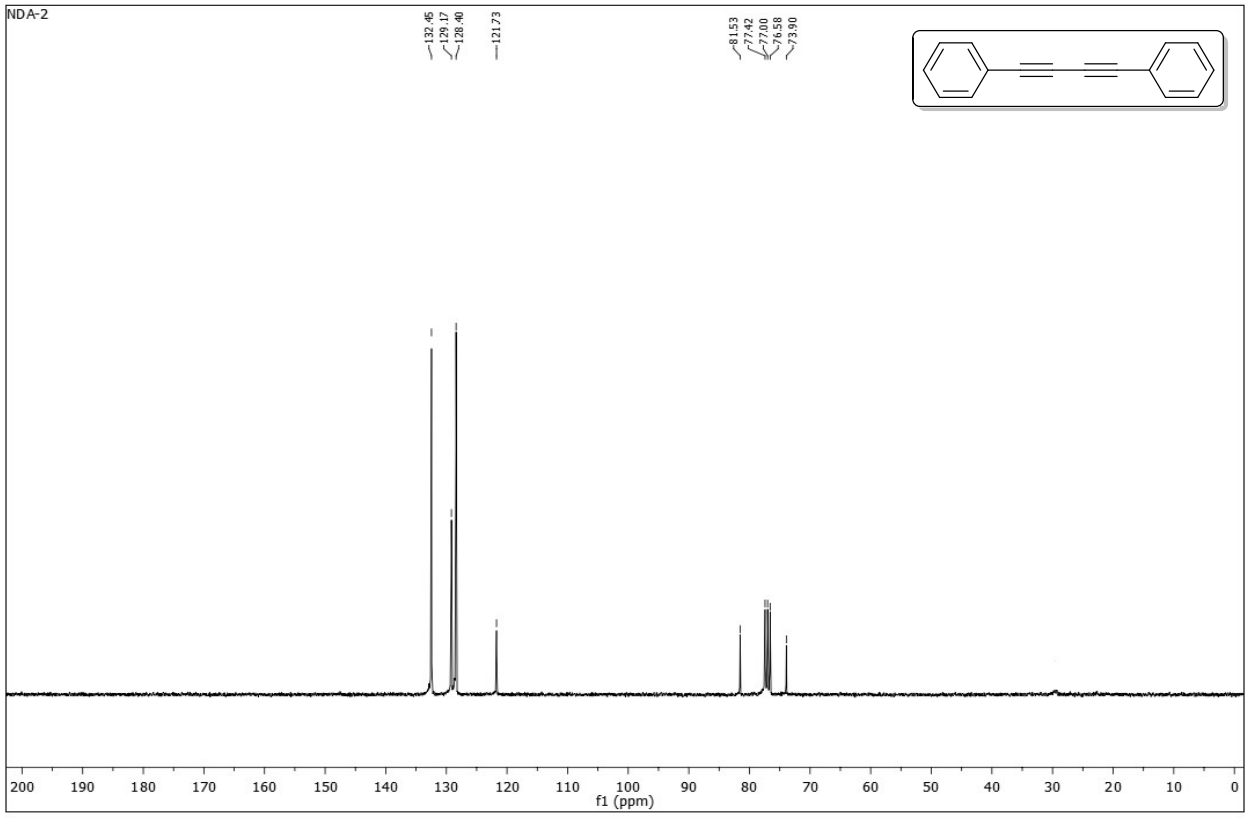

Fig. S20 ^{13}C NMR spectrum of 1,4-diphenylbuta-1,3-diyne **3a** (75 MHz, $CDCl_3$)

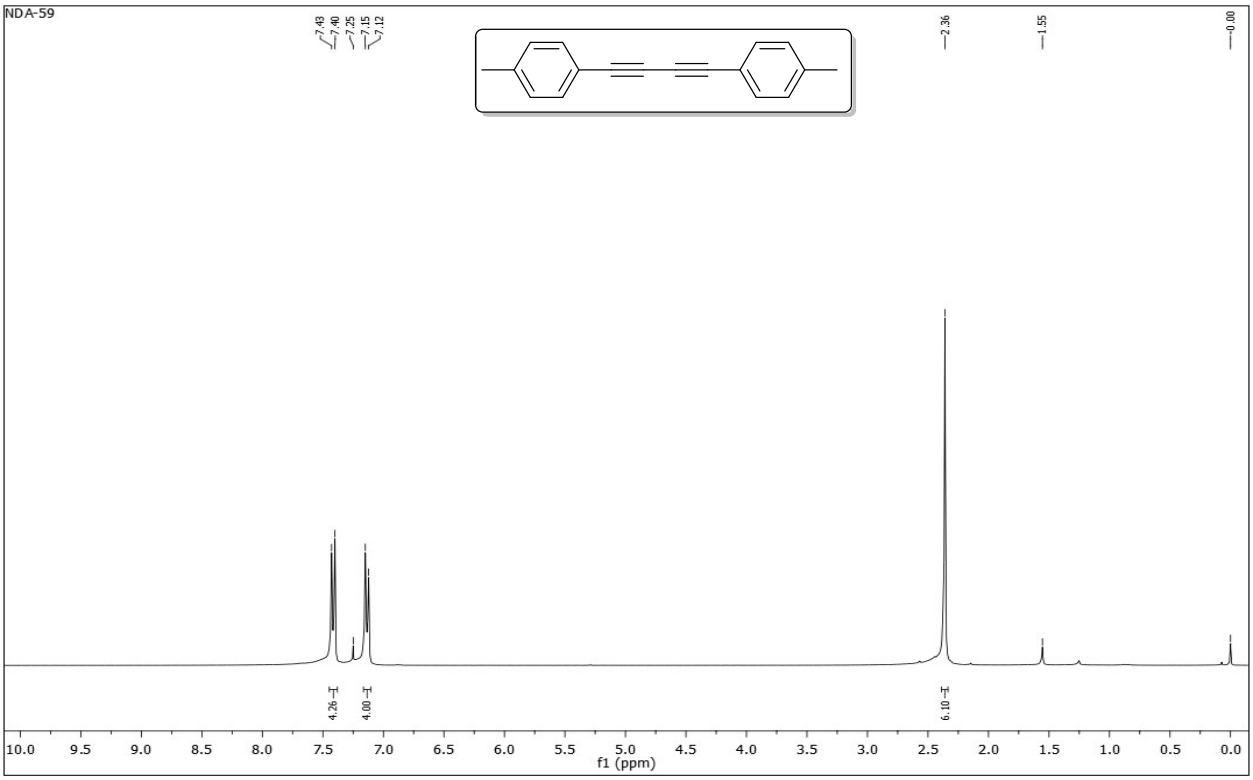

Fig. S21 ^{1}H NMR spectrum of 1,4-di-*p*-tolylbuta-1,3-diyne **(3b)** (300 MHz, $CDCl_3$)

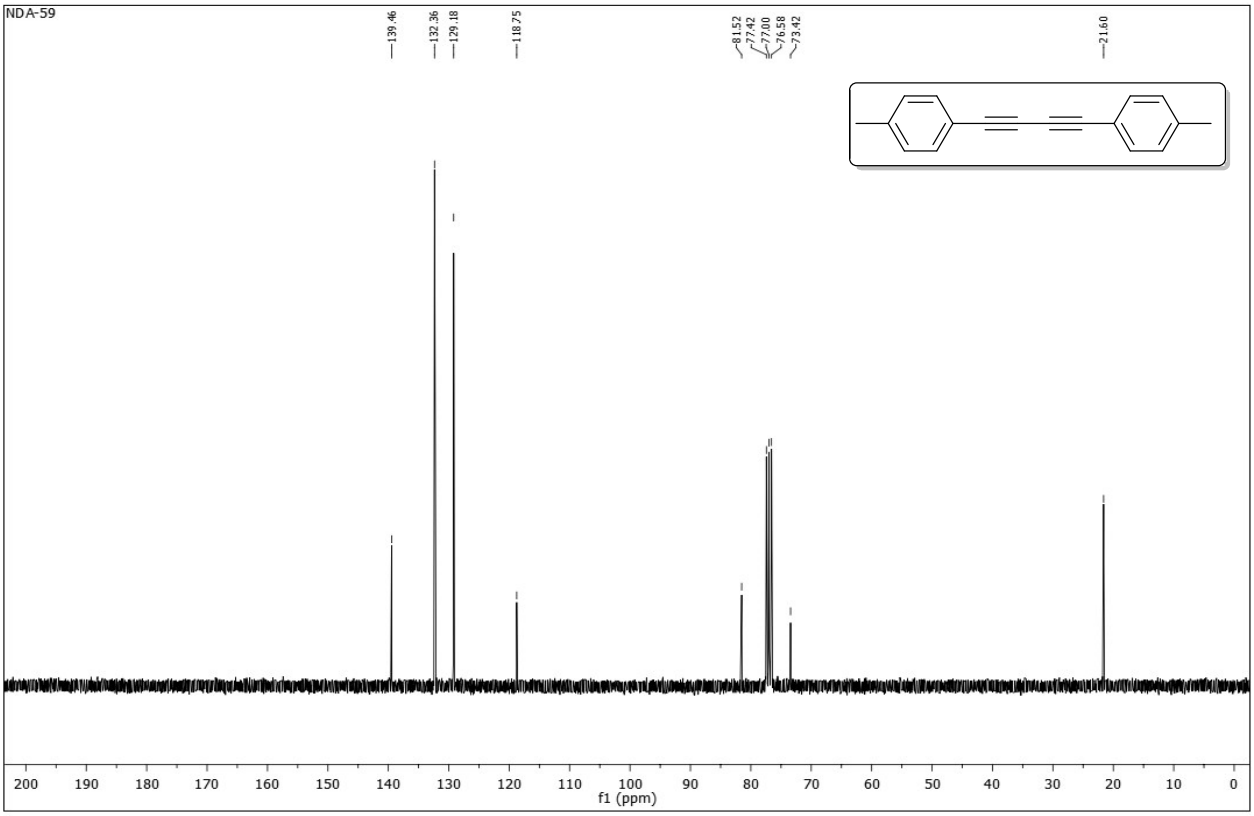

Fig. S22 ^{13}C NMR spectrum of 1,4-di-*p*-tolylbuta-1,3-diyne **(3b)** (75 MHz, $CDCl_3$)

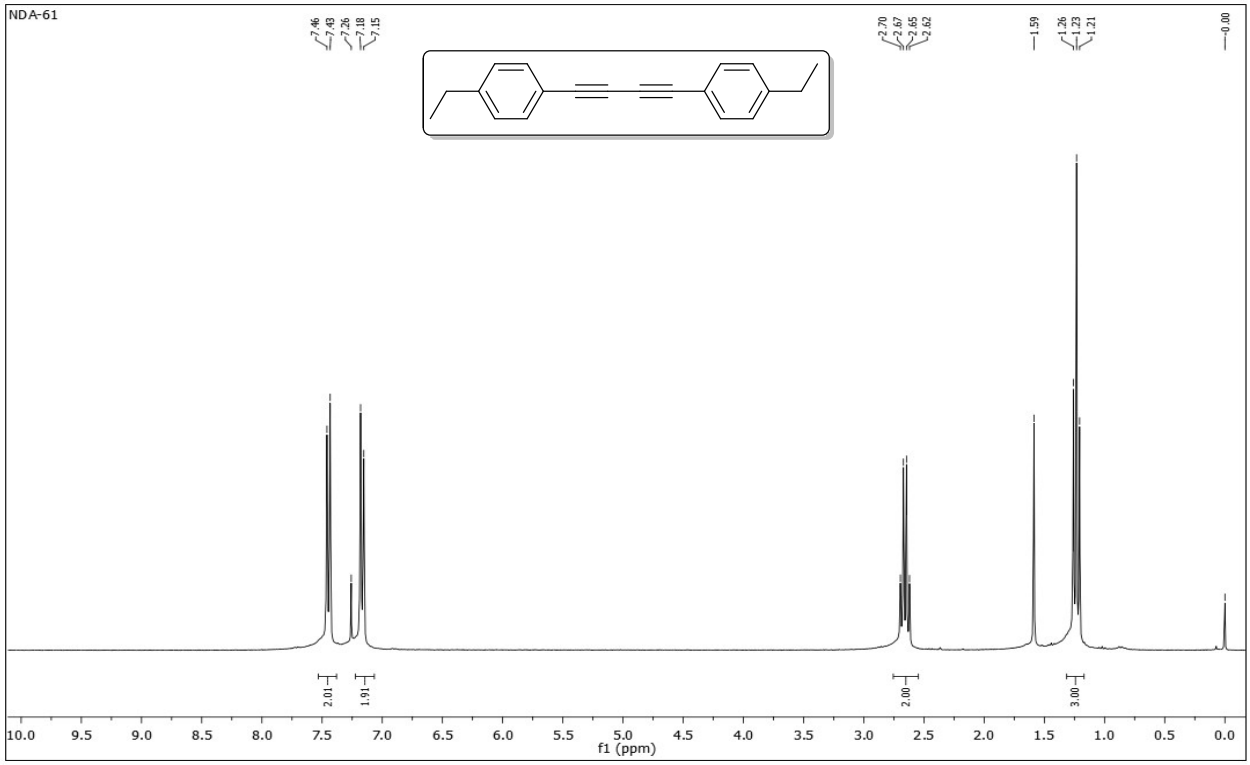

Fig. S23 ^{1}H NMR spectrum of 1,4-bis(4-ethylphenyl)buta-1,3-diyne **(3c)** (300 MHz, $CDCl_3$)

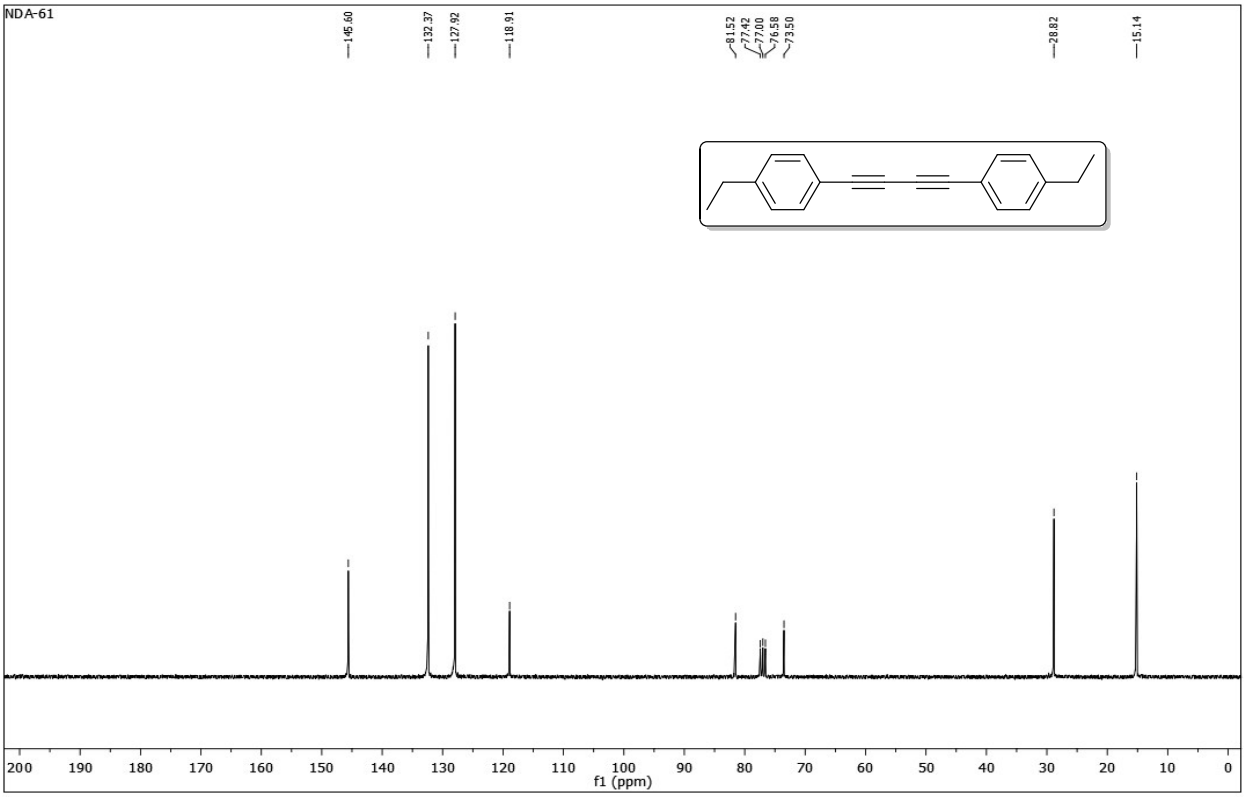

Fig. S24 ^{13}C NMR spectrum of 1,4-bis(4-ethylphenyl)buta-1,3-diyne **(3c)** (75 MHz, $CDCl_3$)

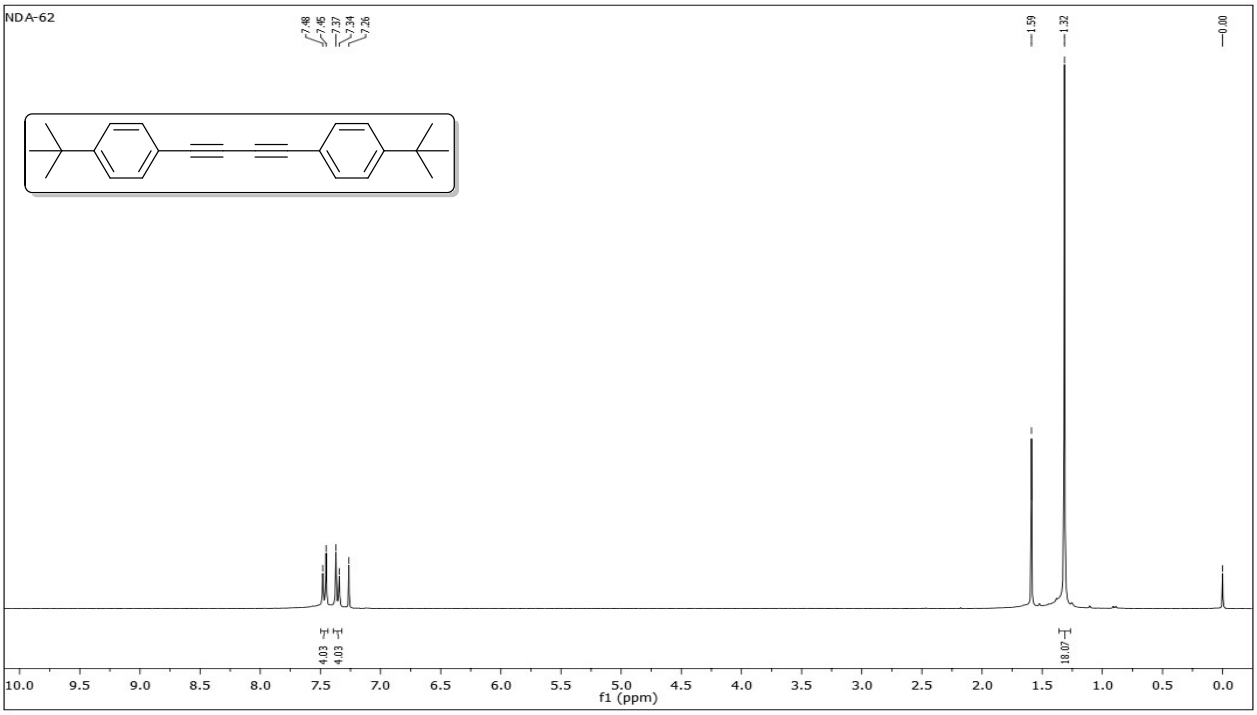

Fig. S25 ^{1}H NMR spectrum of 1,4-bis(4-(*tert*-butyl)phenyl)buta-1,3-diyne (**3d)** (300 MHz, $CDCl_3$)

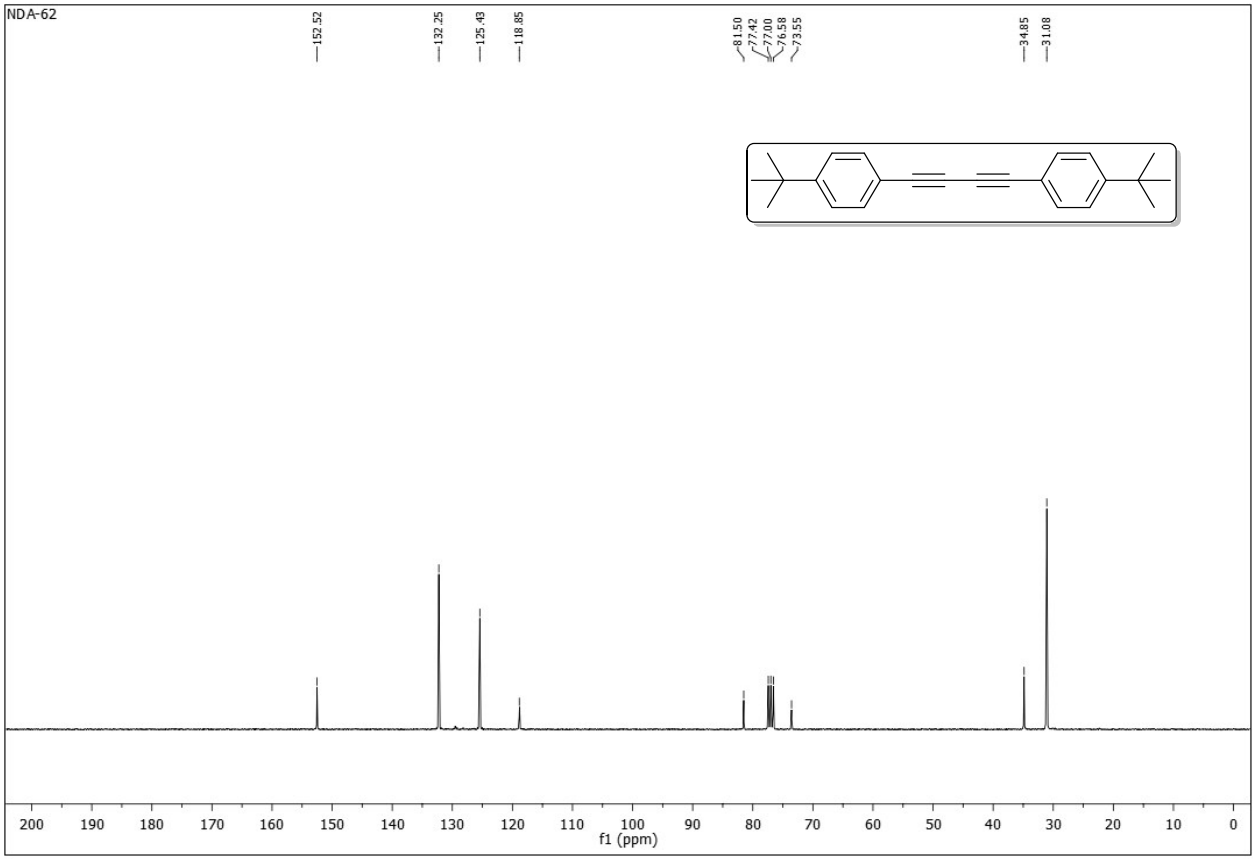

Fig. S26 ^{13}C NMR spectrum of 1,4-bis(4-(*tert*-butyl)phenyl)buta-1,3-diyne (**3d)** (75 MHz, $CDCl_3$)

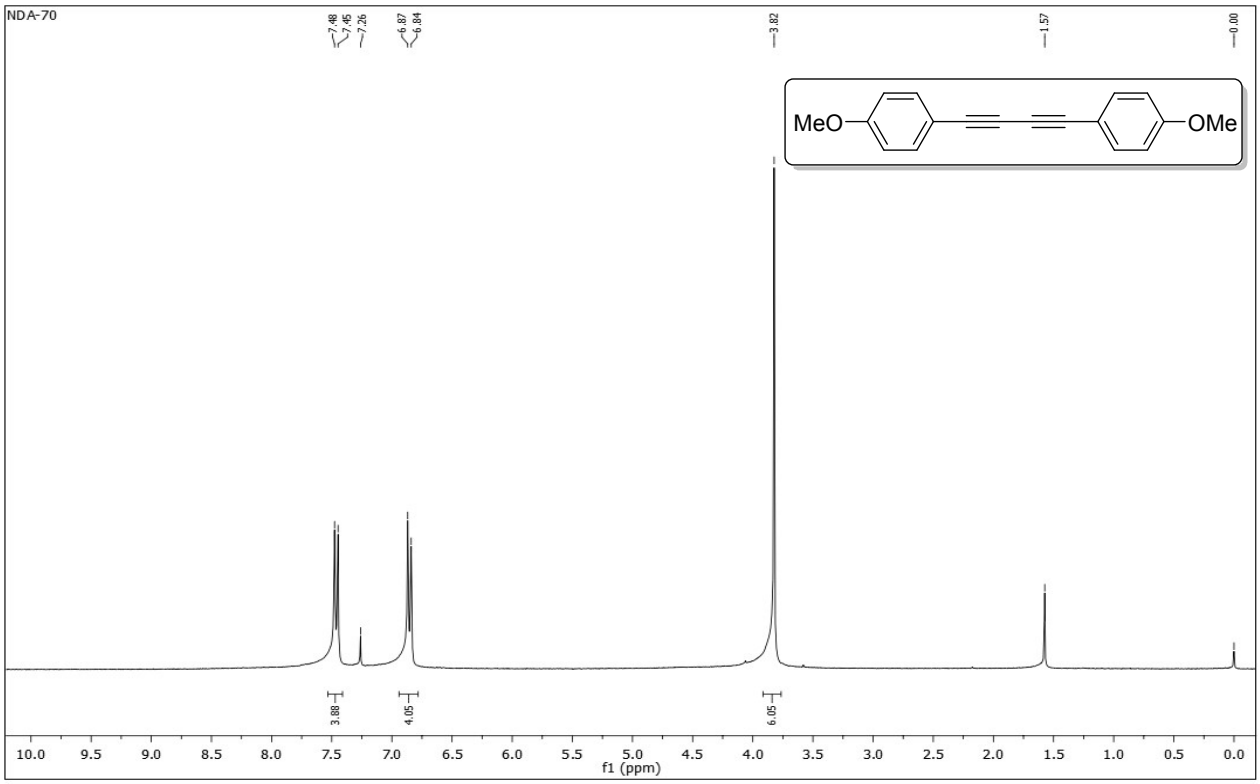

Fig. S27 ^{1}H NMR spectrum of 1,4-bis(4-methoxyphenyl)buta-1,3-diyne **(3e)** (300 MHz, $CDCl_3$)

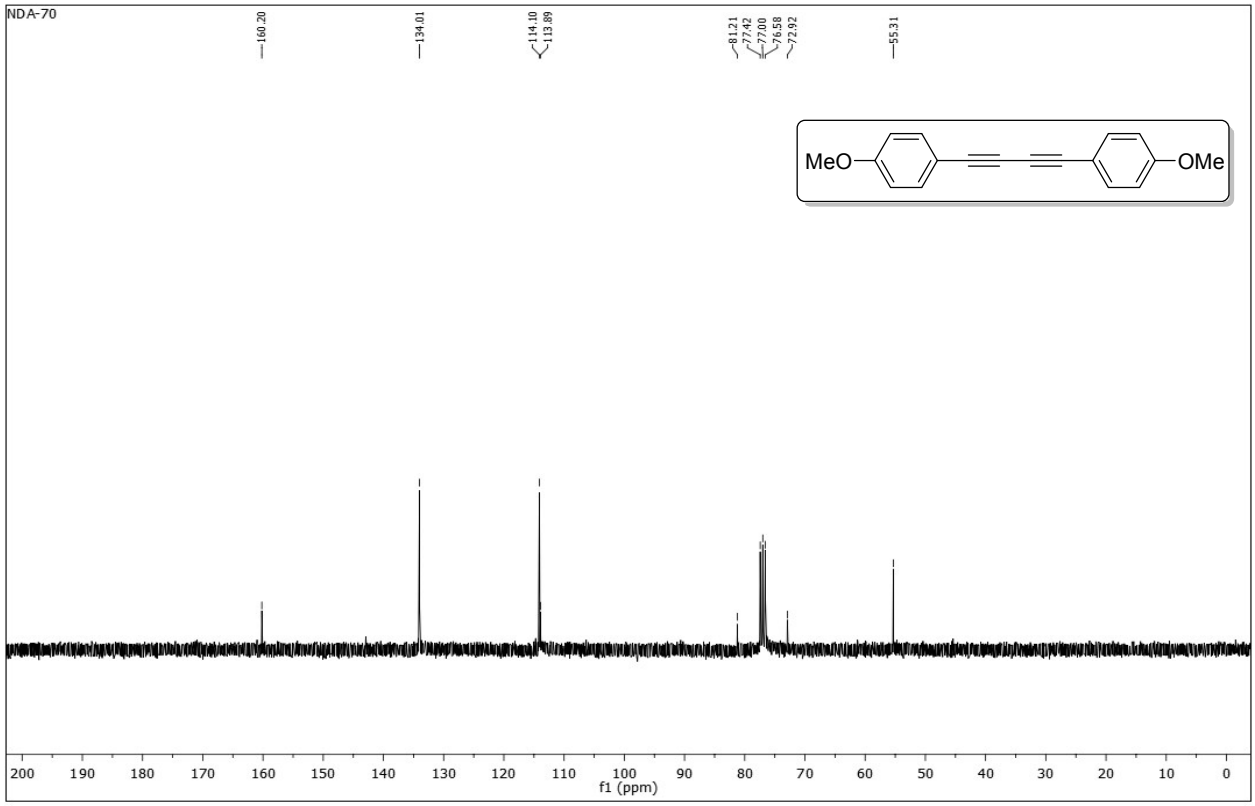

Fig. S28 ^{13}C NMR spectrum of 1,4-bis(4-methoxyphenyl)buta-1,3-diyne **(3e)** (75 MHz, $CDCl_3$)

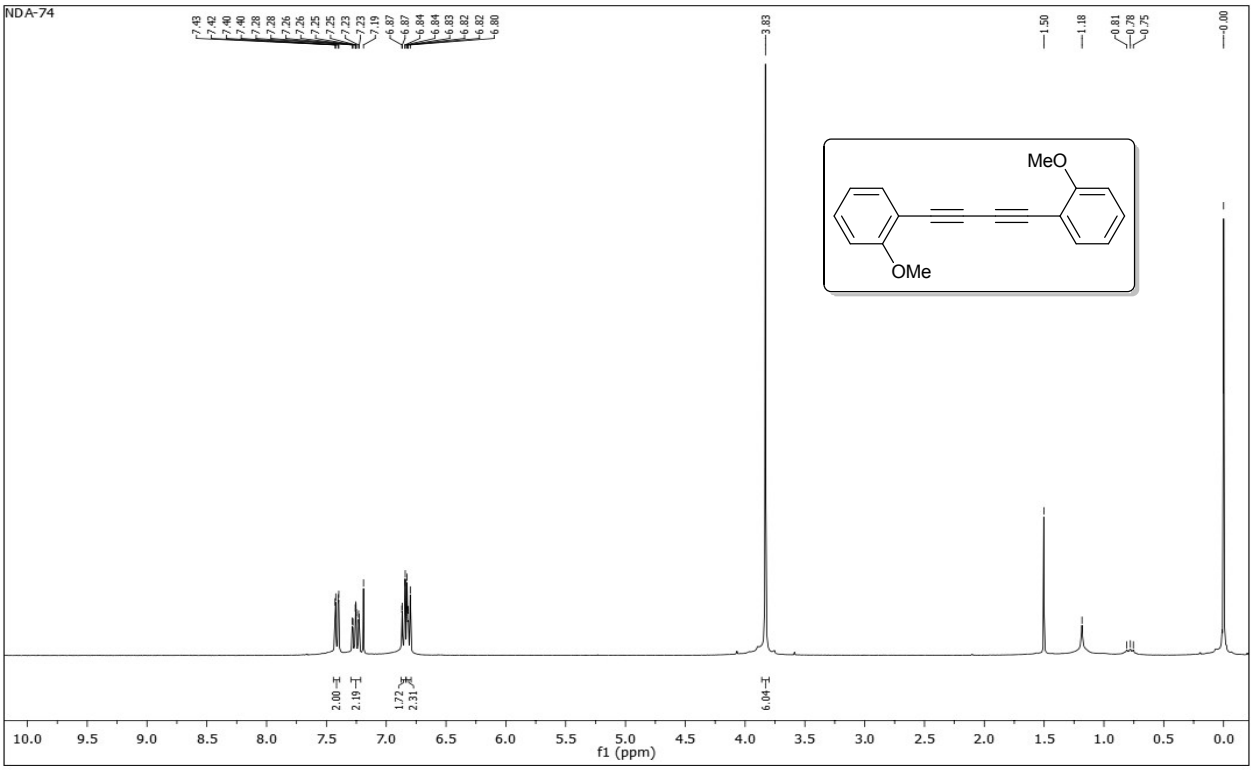

Fig. S29 ^{1}H NMR spectrum of 1,4-bis(2-methoxyphenyl)buta-1,3-diyne **(3f)** (300 MHz, $CDCl_3$)

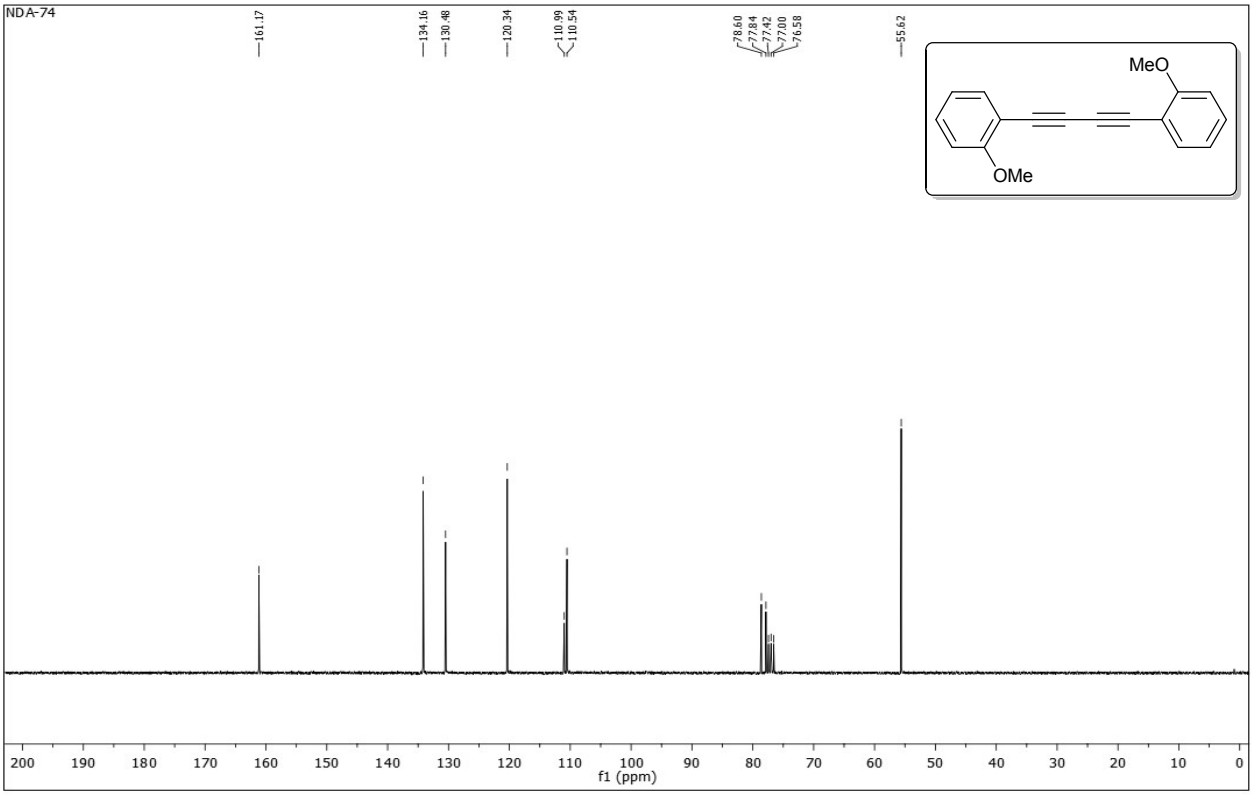

Fig. S30 ^{13}C NMR spectrum of 1,4-bis(2-methoxyphenyl)buta-1,3-diyne **(3f)** (75 MHz, $CDCl_3$)

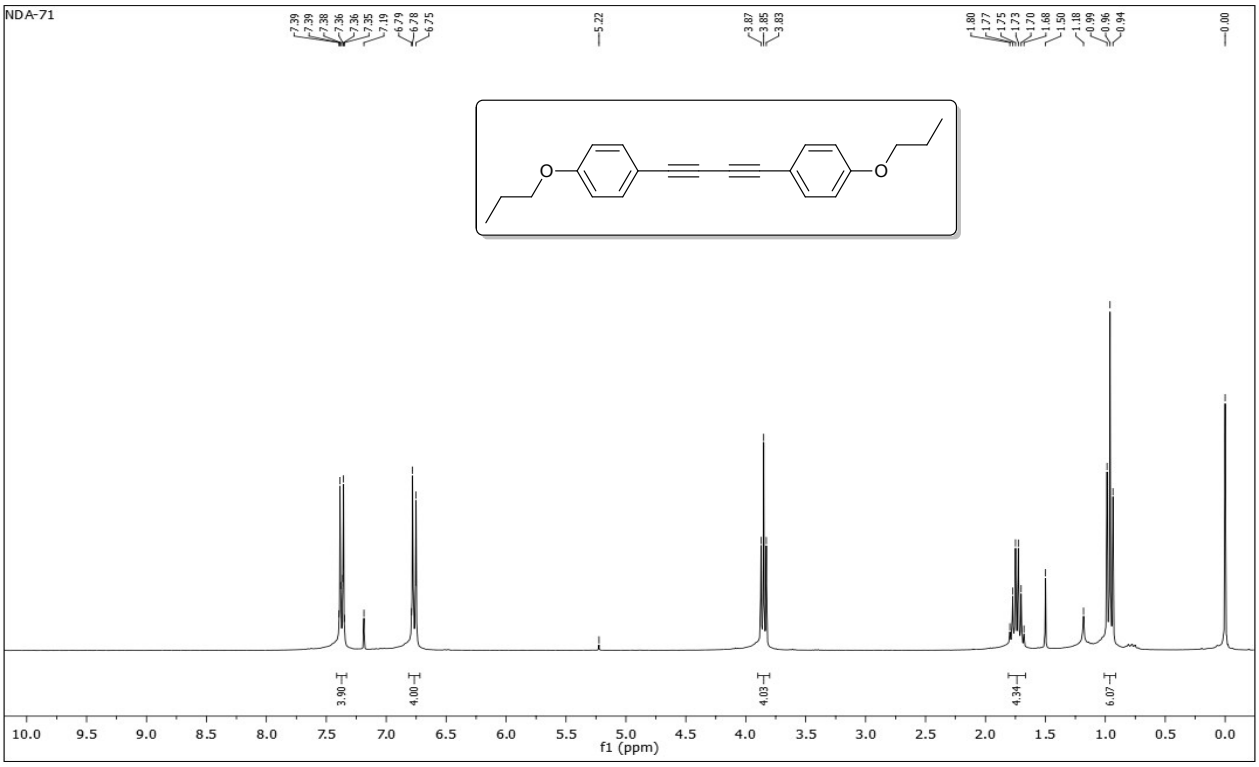

Fig. S31 ^{1}H NMR spectrum of 1,4-bis(4-propoxyphenyl)buta-1,3-diyne **(3g)** (300 MHz, $CDCl_3$)

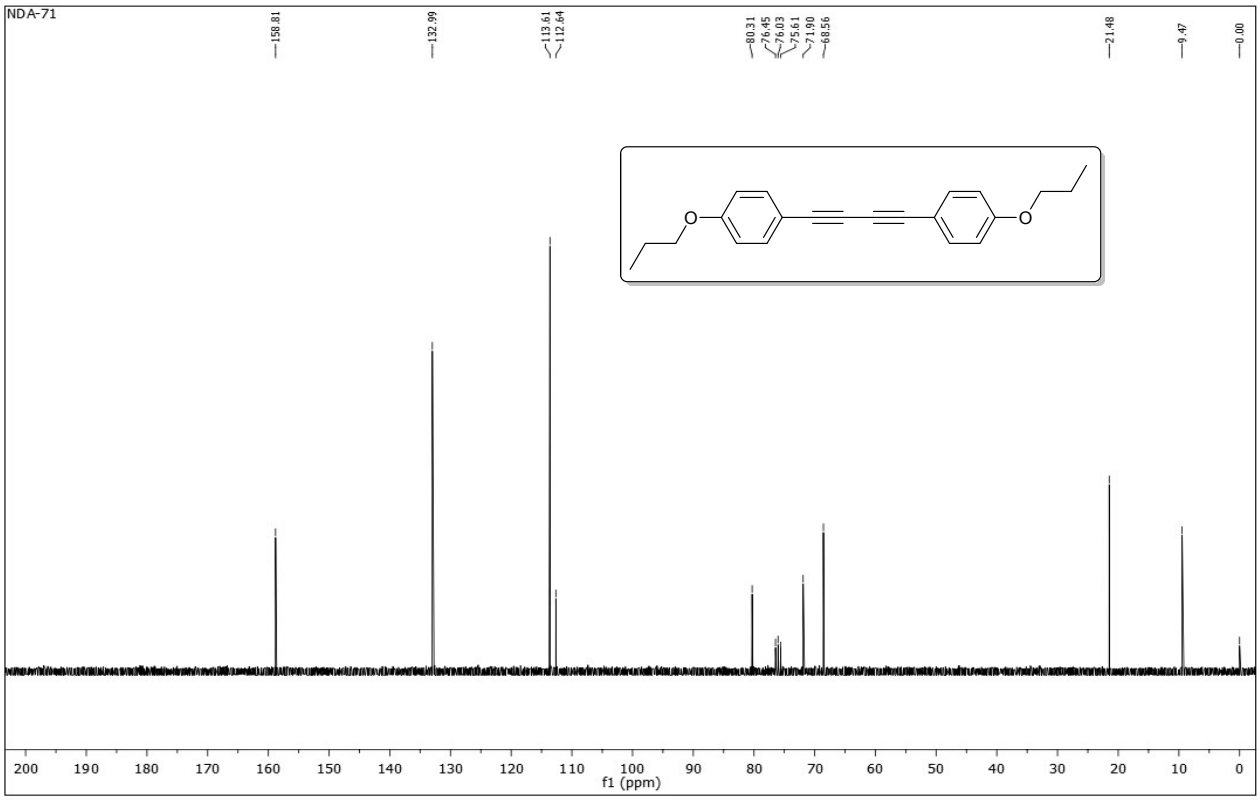

Fig. S32 ^{13}C NMR spectrum of 1,4-bis(4-propoxyphenyl)buta-1,3-diyne **(3g)** (75 MHz, $CDCl_3$)

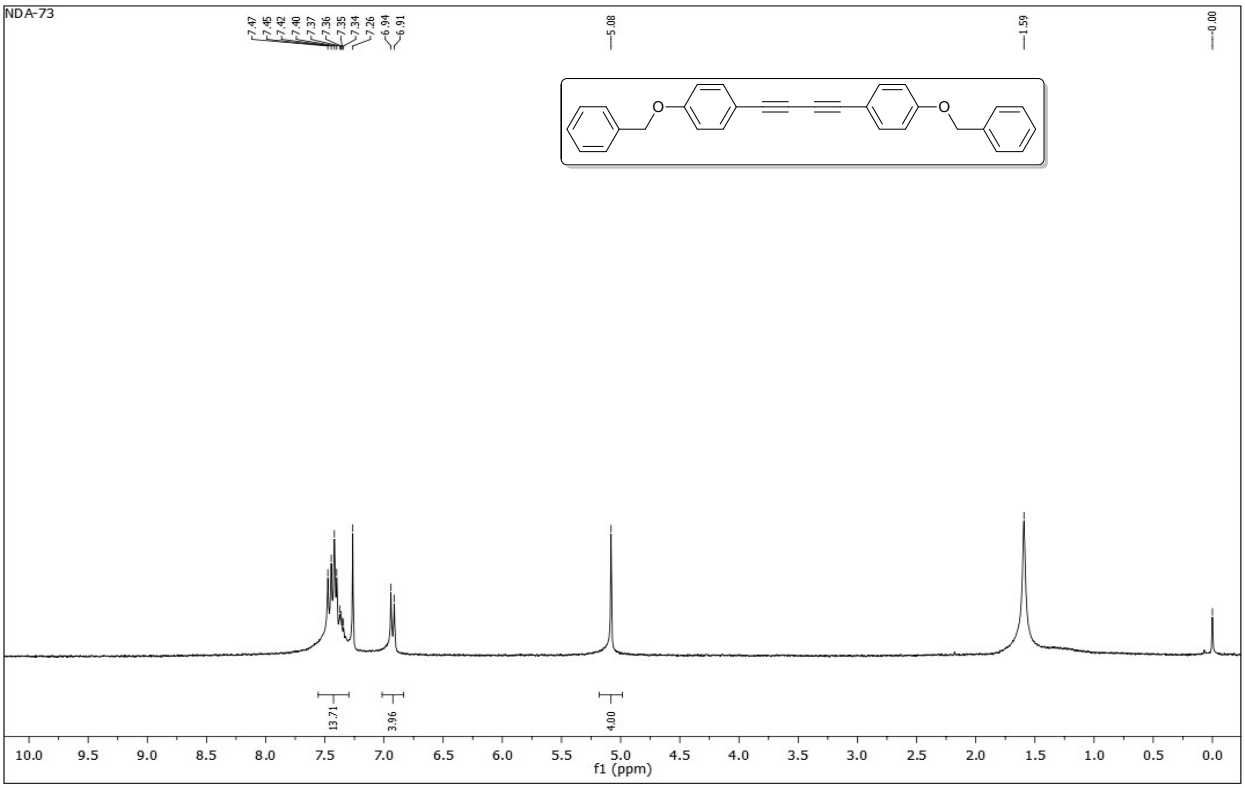

Fig. S33 ^{1}H NMR spectrum of 1,4-bis(4-(benzyloxy)phenyl)buta-1,3-diyne **(3h)** (300 MHz, $CDCl_3$)

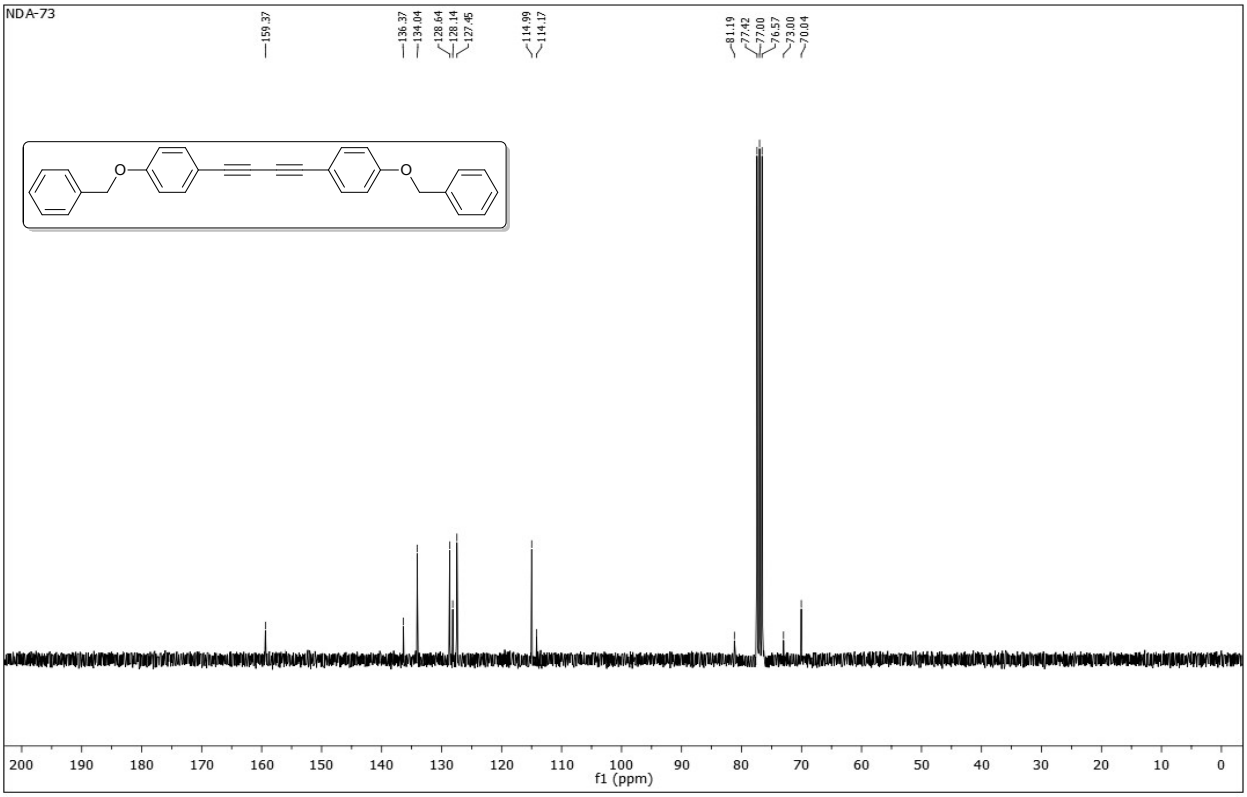

Fig. S34 ^{13}C NMR spectrum of 1,4-bis(4-(benzyloxy)phenyl)buta-1,3-diyne **(3h)** (75 MHz, $CDCl_3$)

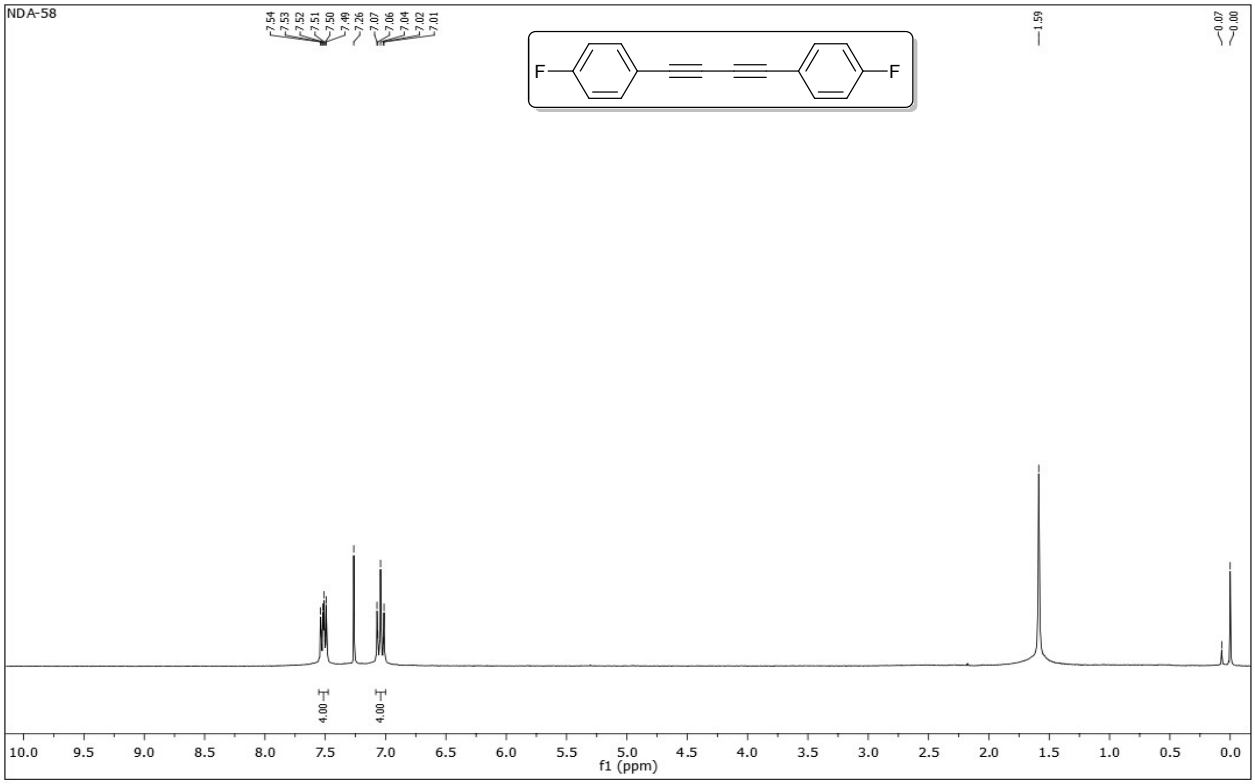

Fig. S35 ^{1}H NMR spectrum of 1,4-bis(4-fluorophenyl)buta-1,3-diyne **(3i)** (300 MHz, $CDCl_3$)

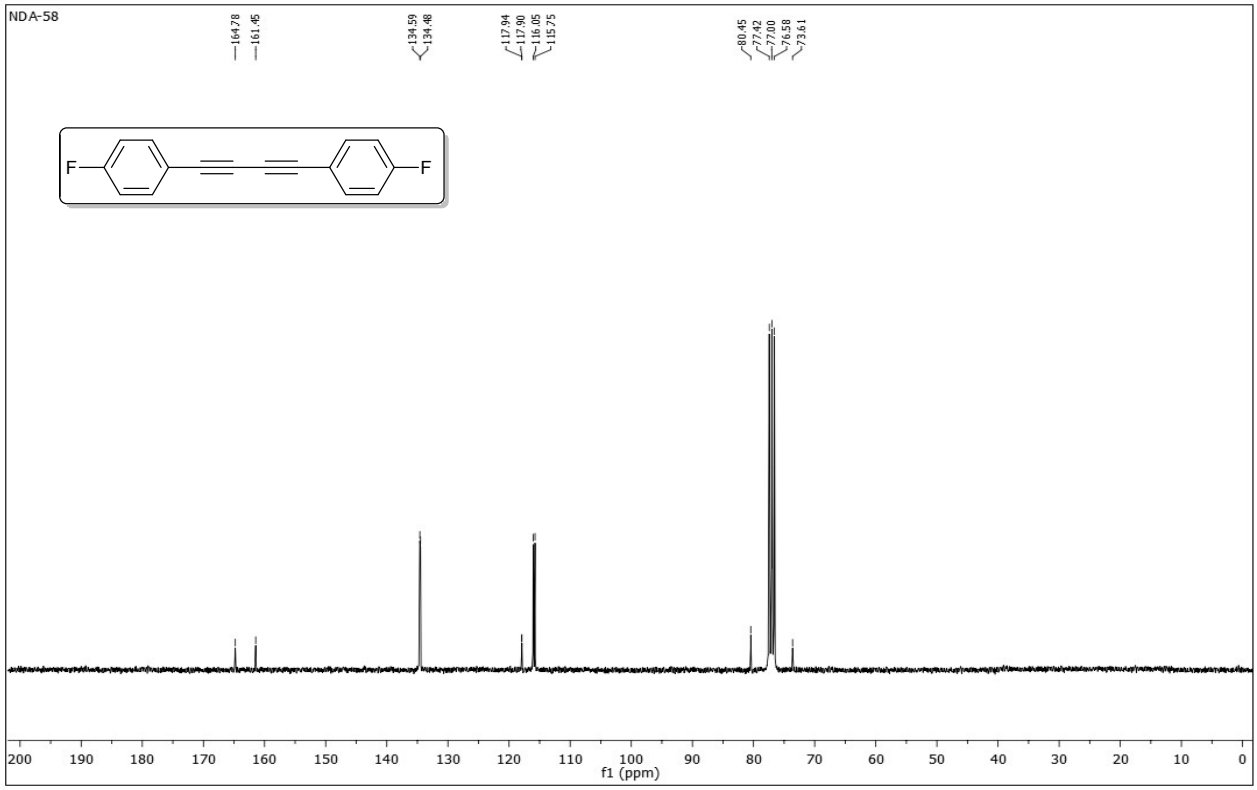

Fig. S36 ^{13}C NMR spectrum of 1,4-bis(4-fluorophenyl)buta-1,3-diyne **(3i)** (75 MHz, $CDCl_3$)

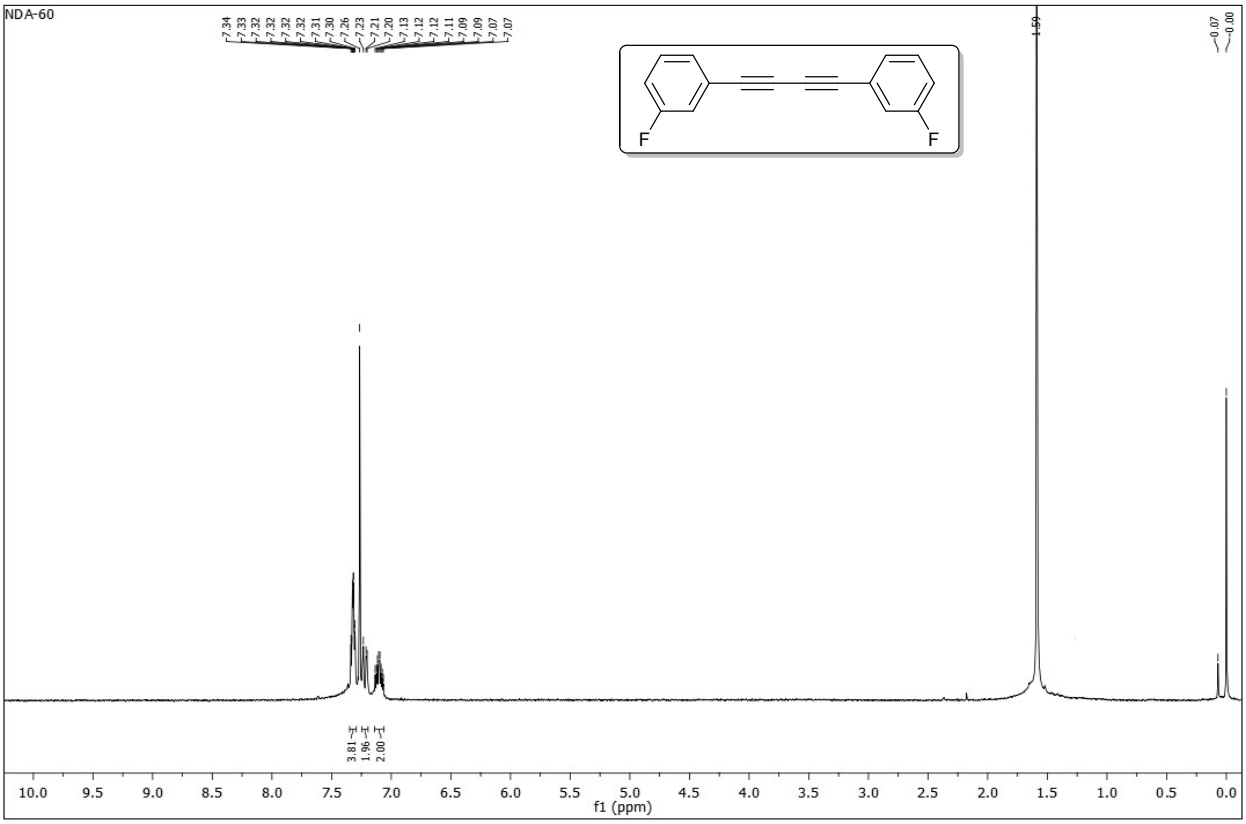

Fig. S37 ^{1}H NMR spectrum of 1,4-bis(3-fluorophenyl)buta-1,3-diyne **(3j)** (300 MHz, $CDCl_3$)

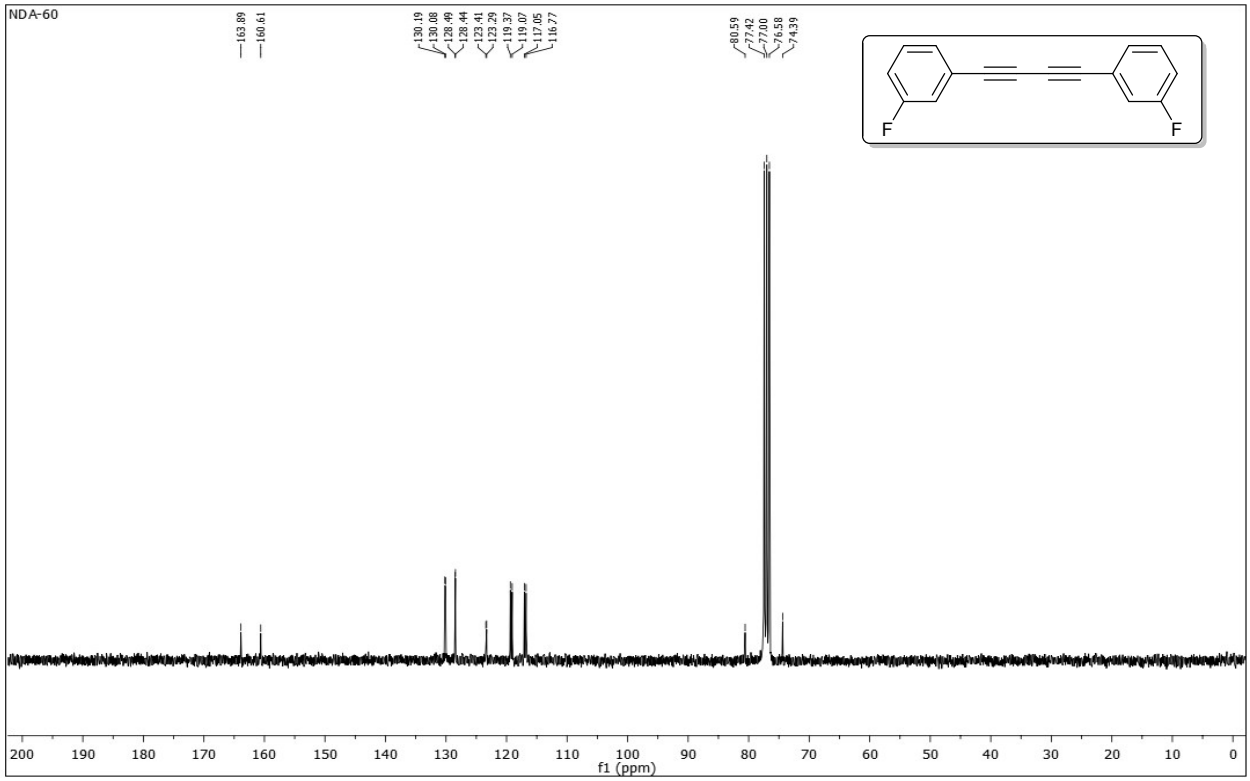

Fig. S38 ^{13}C NMR spectrum of 1,4-bis(3-fluorophenyl)buta-1,3-diyne **(3j)** (75 MHz, $CDCl_3$)

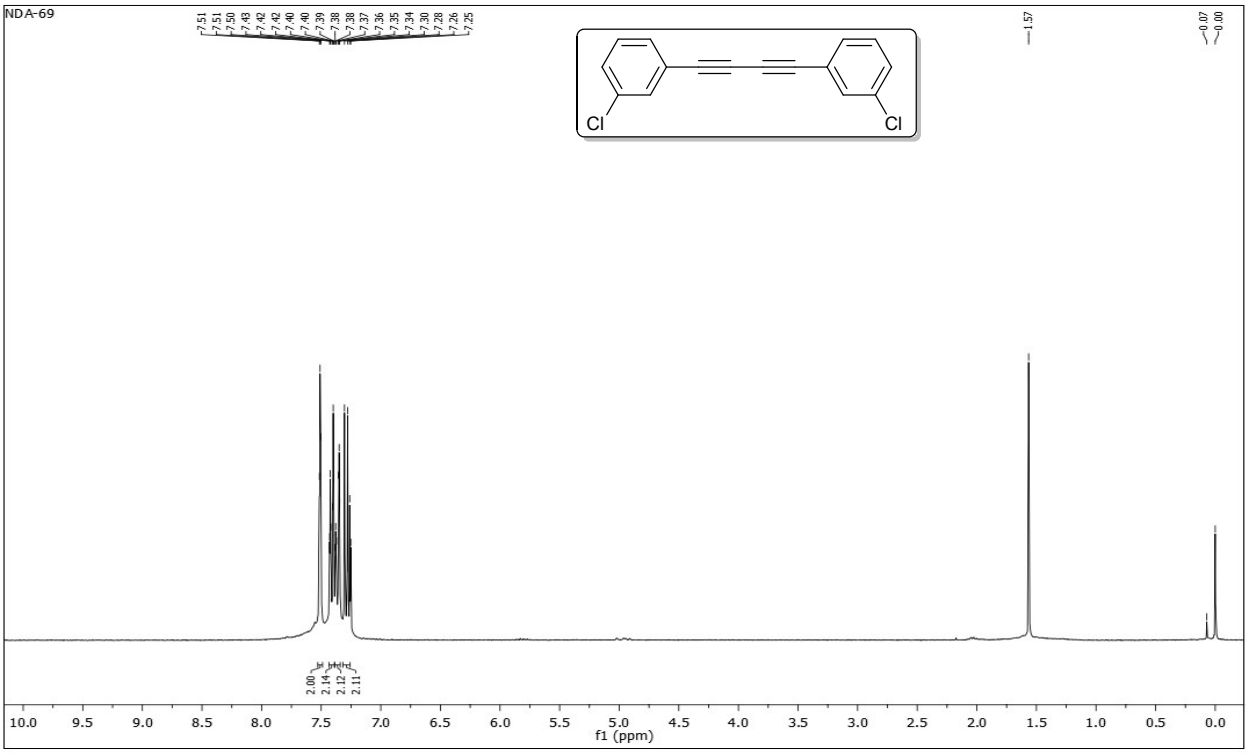

Fig. S39 ^{1}H NMR spectrum of 1,4-bis(3-chlorophenyl)buta-1,3-diyne **(3k)** (300 MHz, $CDCl_3$)

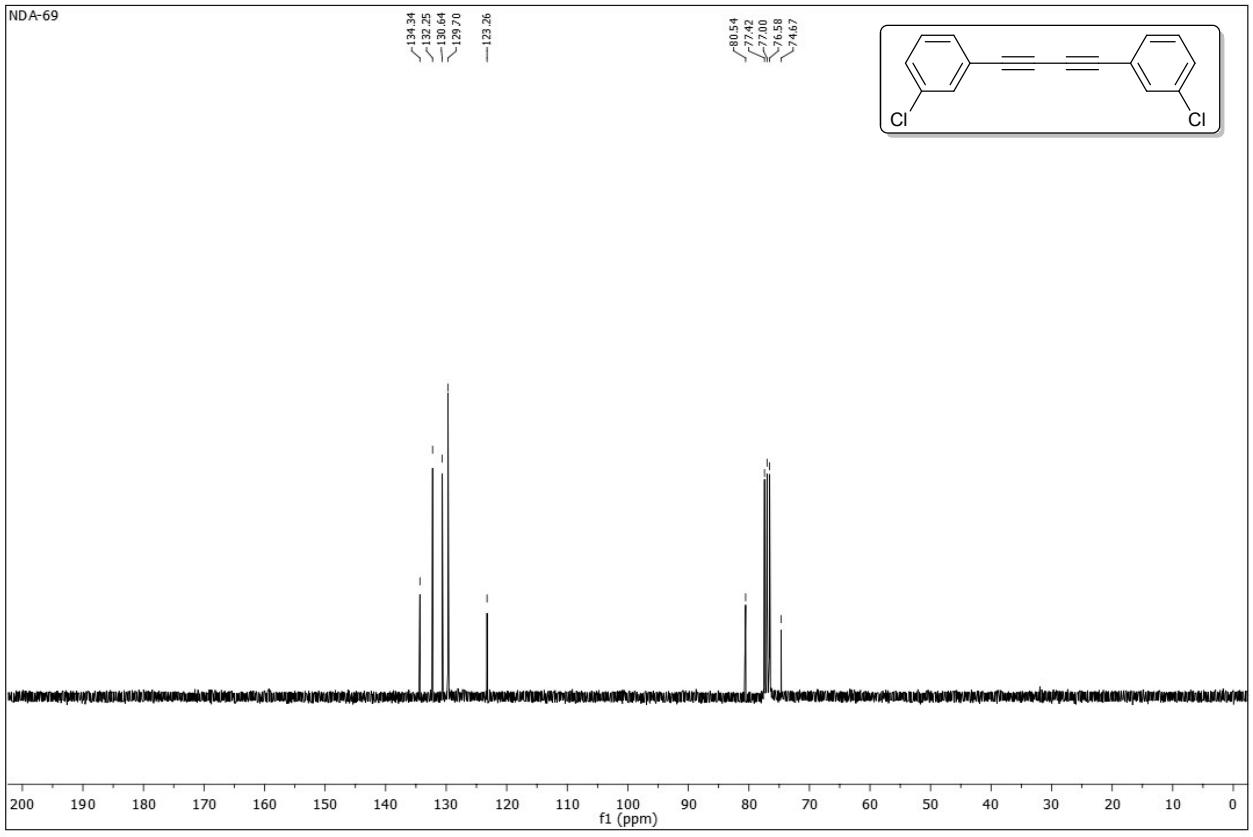

Fig. S40 ^{13}C NMR spectrum of 1,4-bis(3-chlorophenyl)buta-1,3-diyne **(3k)** (75 MHz, $CDCl_3$)

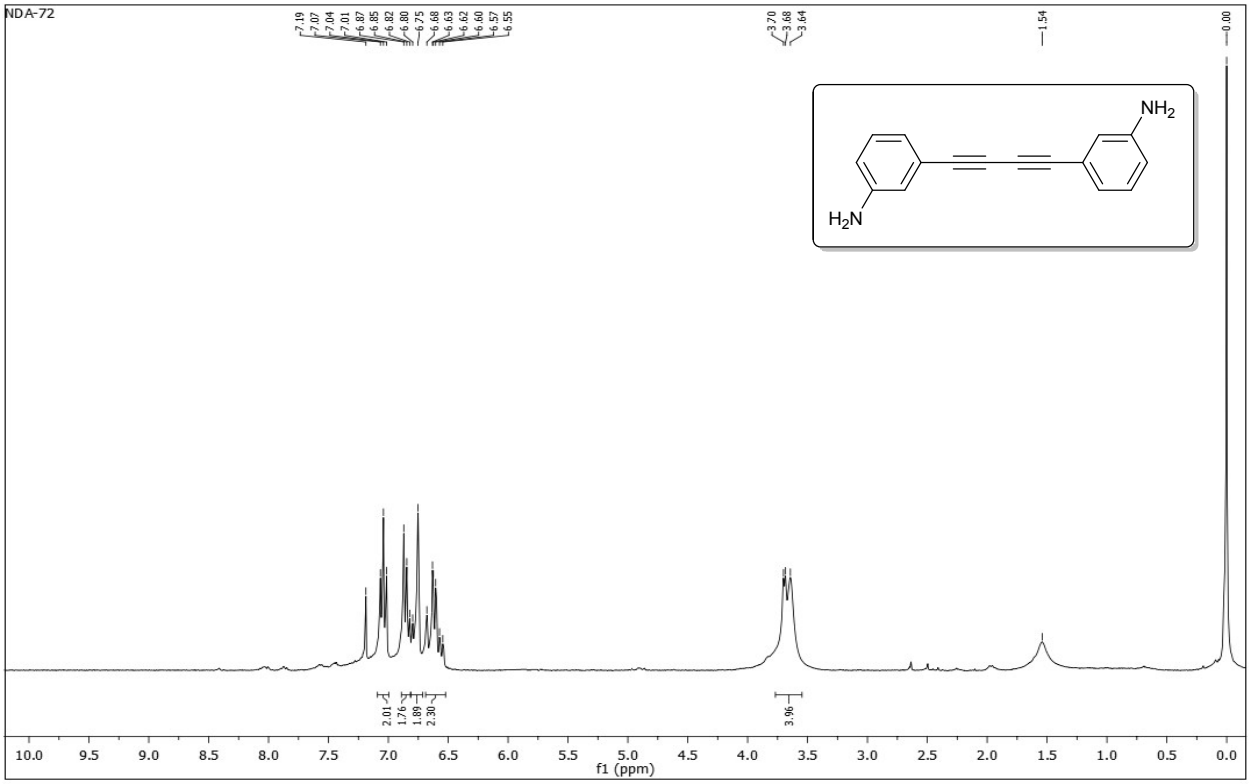

Fig. S41 ^{1}H NMR spectrum of 3,3'-(buta-1,3-diyne-1,4-diyl)dianiline **(3l)** (300 MHz, $CDCl_3$)

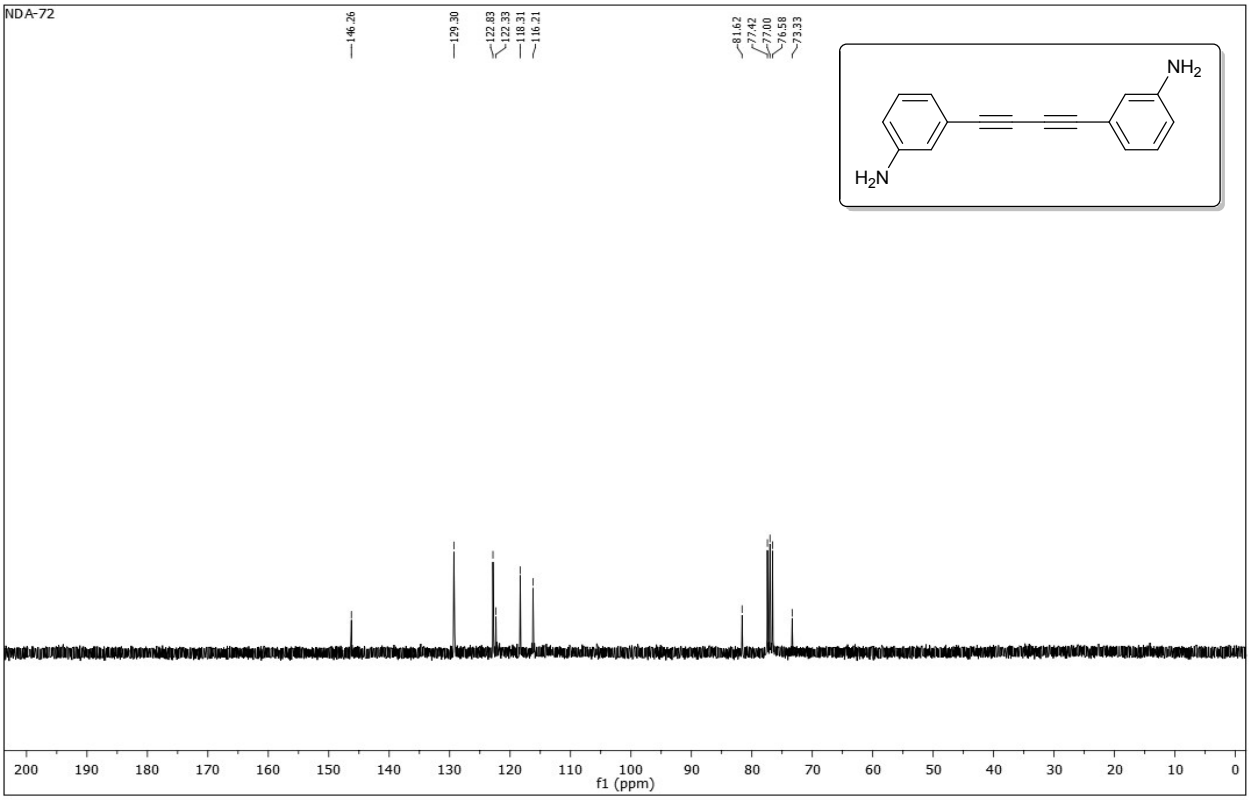

Fig. S42 ^{13}C NMR spectrum of 3,3'-(buta-1,3-diyne-1,4-diyl)dianiline **(3l)** (75 MHz, $CDCl_3$)

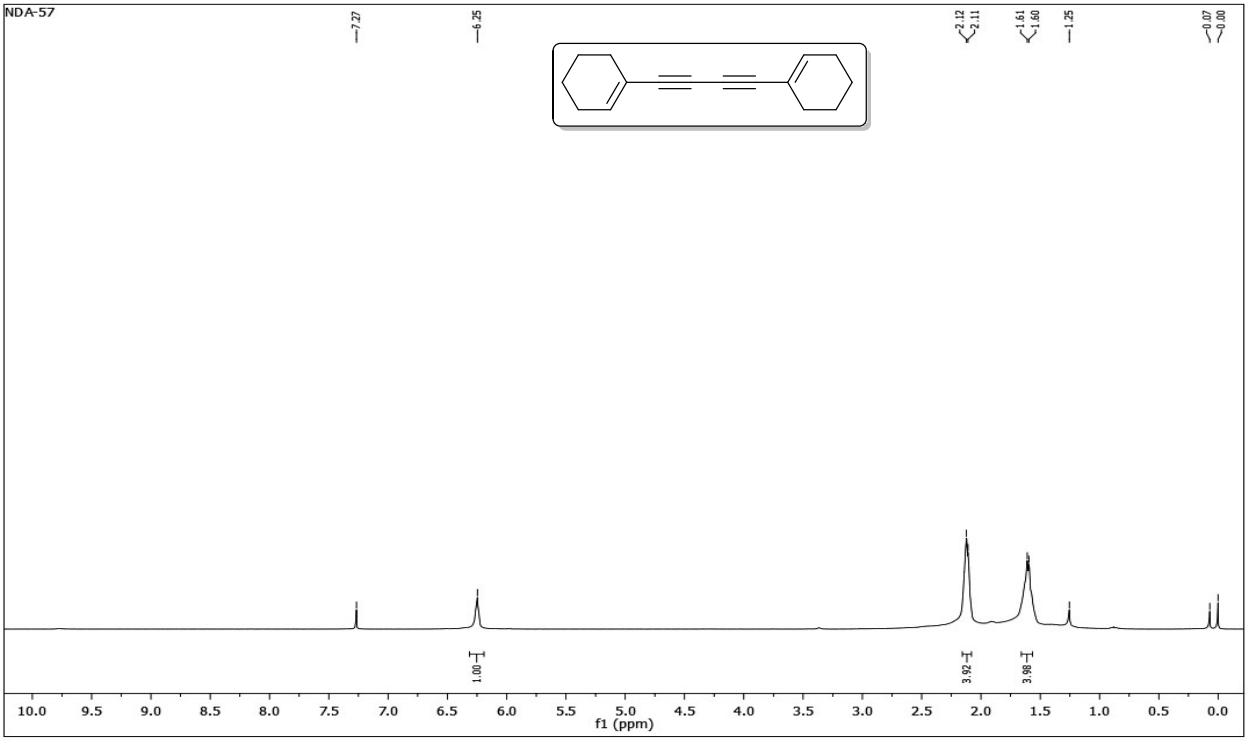

Fig. S43 ^{1}H NMR spectrum of 3,3'-(buta-1,3-diyne-1,4-diyl)dianiline **(3l)** (300 MHz, $CDCl_3$)

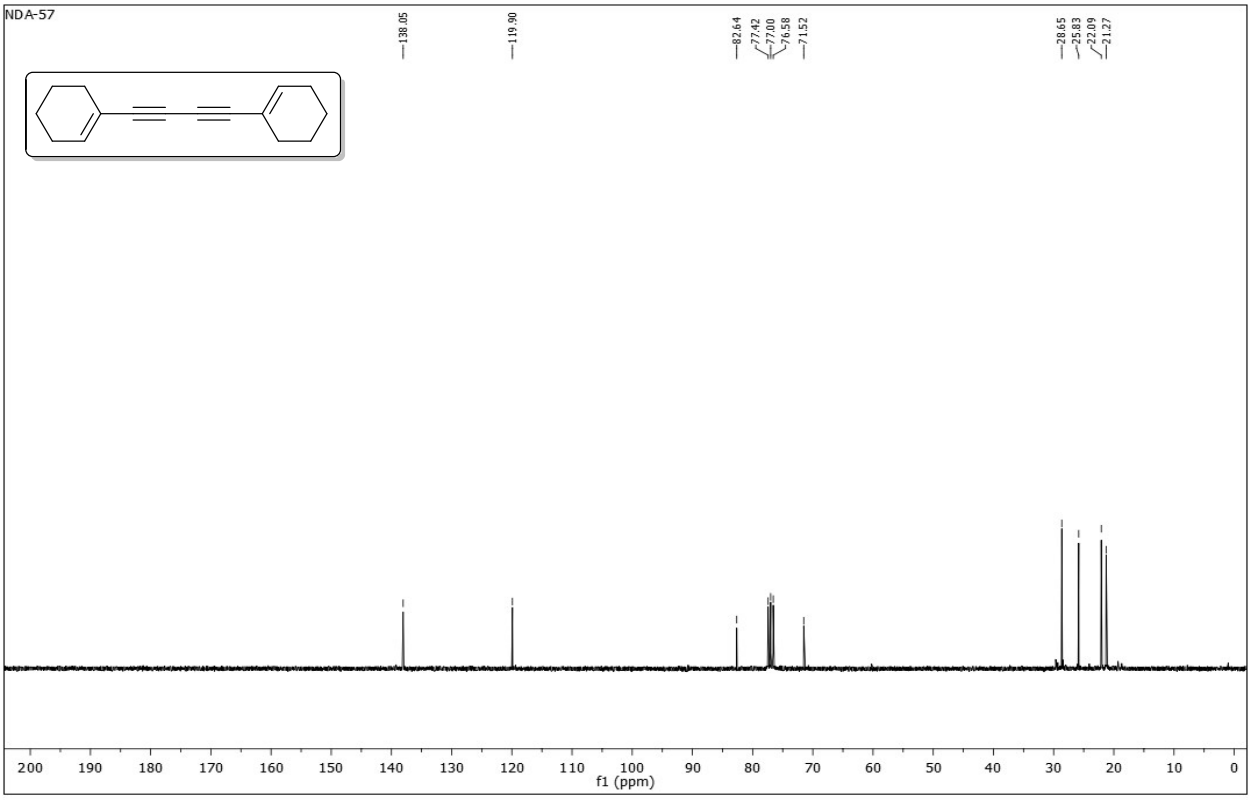

Fig. S44 ^{13}C NMR spectrum of 3,3'-(buta-1,3-diyne-1,4-diyl)dianiline **(3l)** (75 MHz, $CDCl_3$)

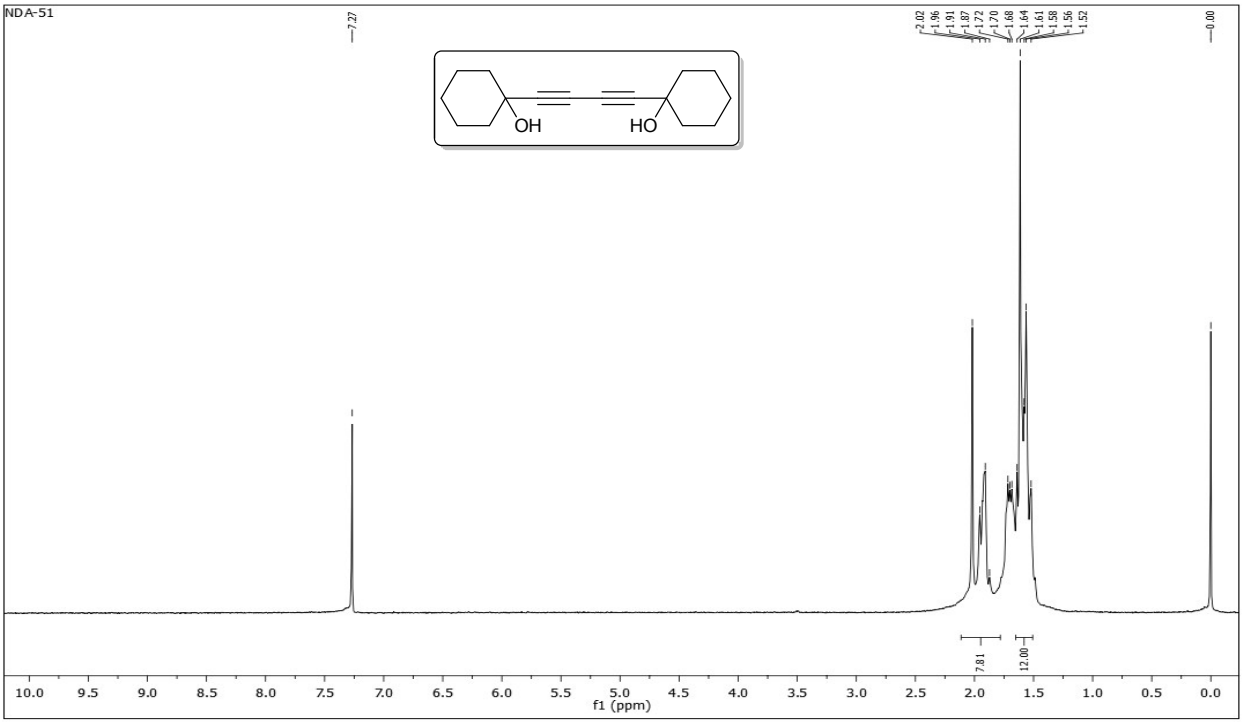

Fig. S45 ^{1}H NMR spectrum of 1,1'-(buta-1,3-diyne-1,4-diyl)dicyclohexanol **(3n)** (300 MHz, $CDCl_3$)

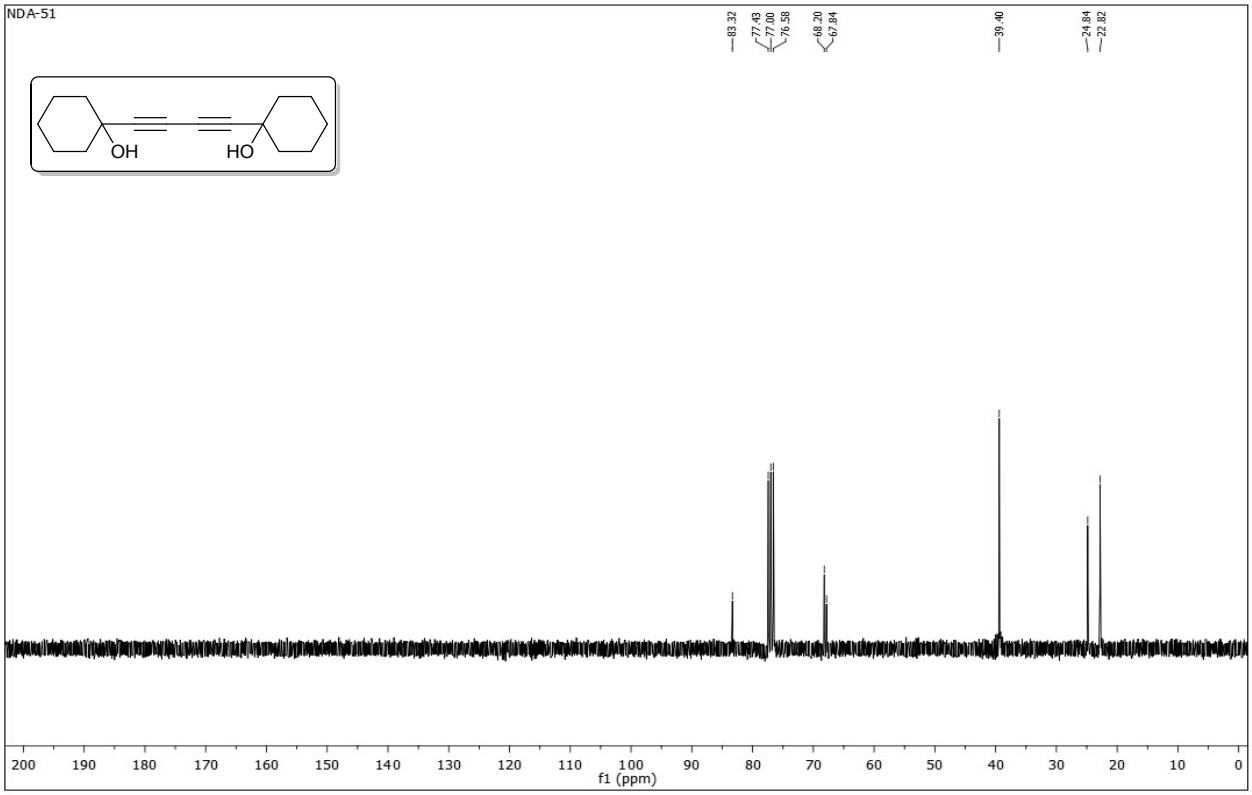

Fig. S46 ^{13}C NMR spectrum of 1,1'-(buta-1,3-diyne-1,4-diyl)dicyclohexanol **(3n)** (75 MHz, $CDCl_3$)

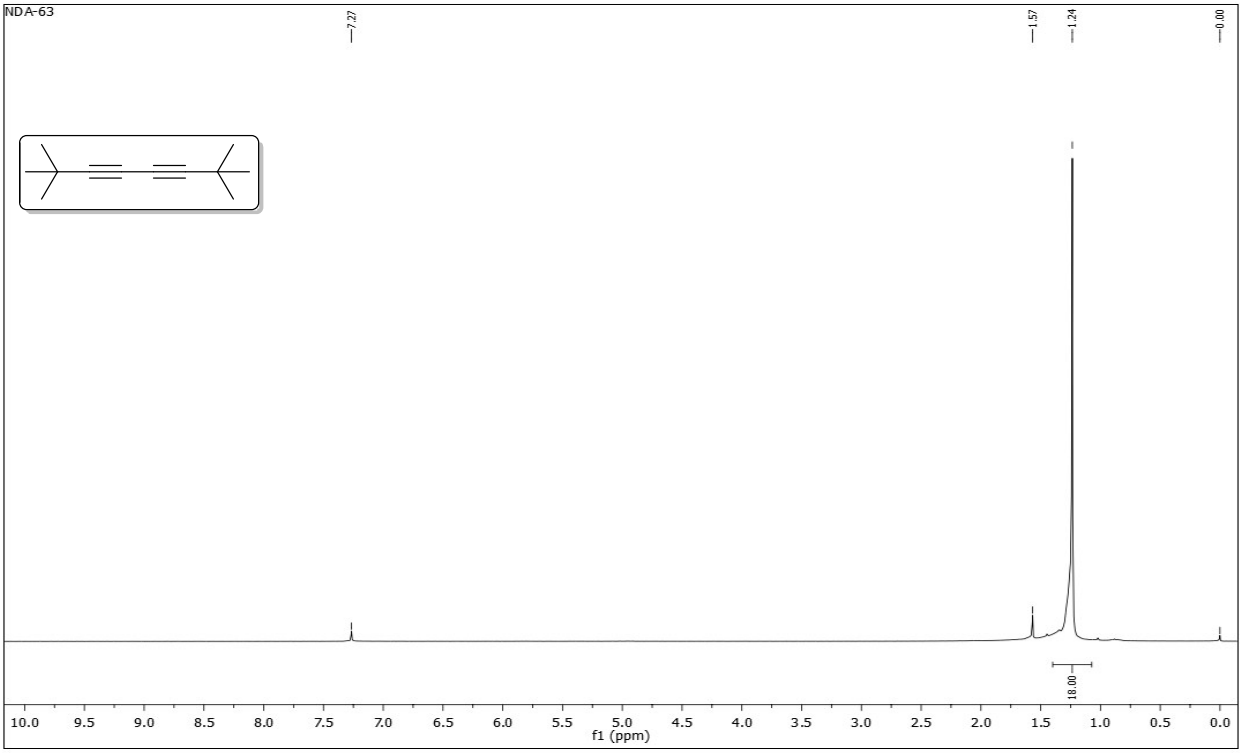

Fig. S47 ^{1}H NMR spectrum of 2,2,7,7-tetramethylocta-3,5-diyne **(3o)** (300 MHz, $CDCl_3$)

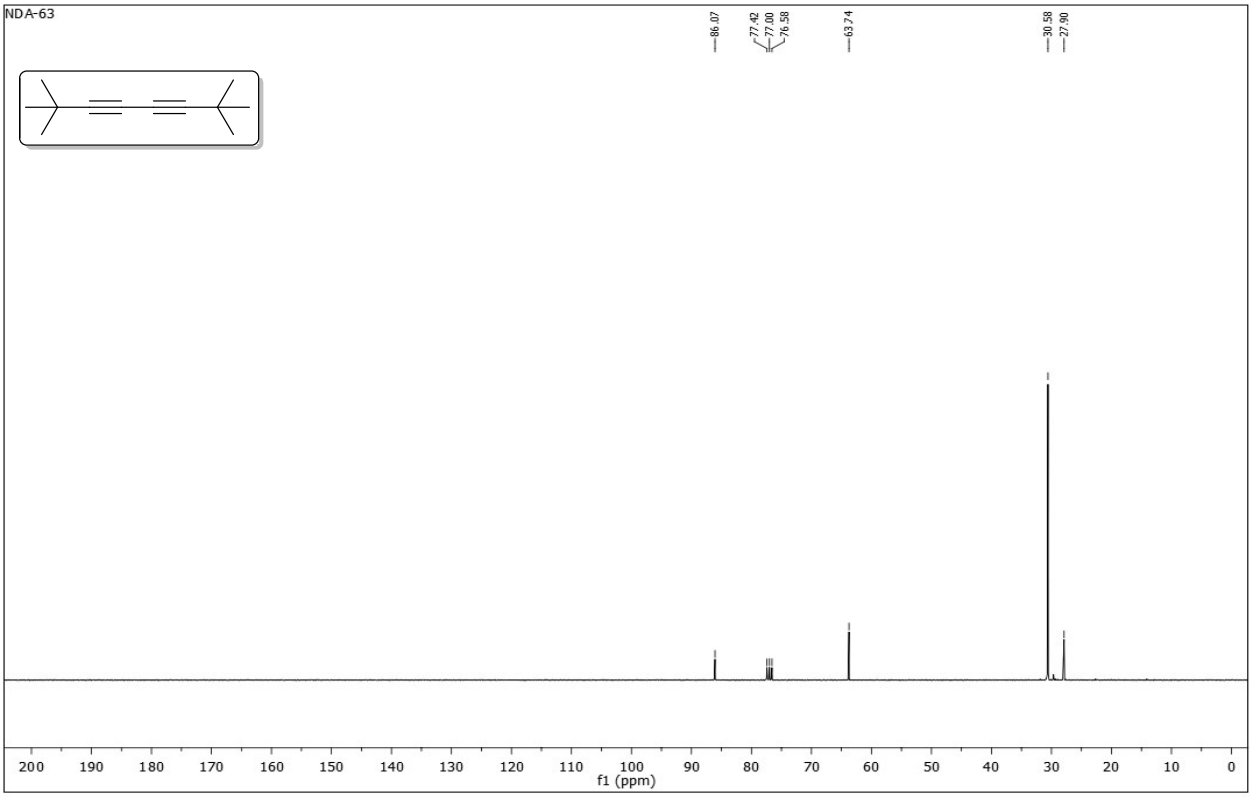

Fig. S48 ^{13}C NMR spectrum of 2,2,7,7-tetramethylocta-3,5-diyne **(3o)** (75 MHz, $CDCl_3$)

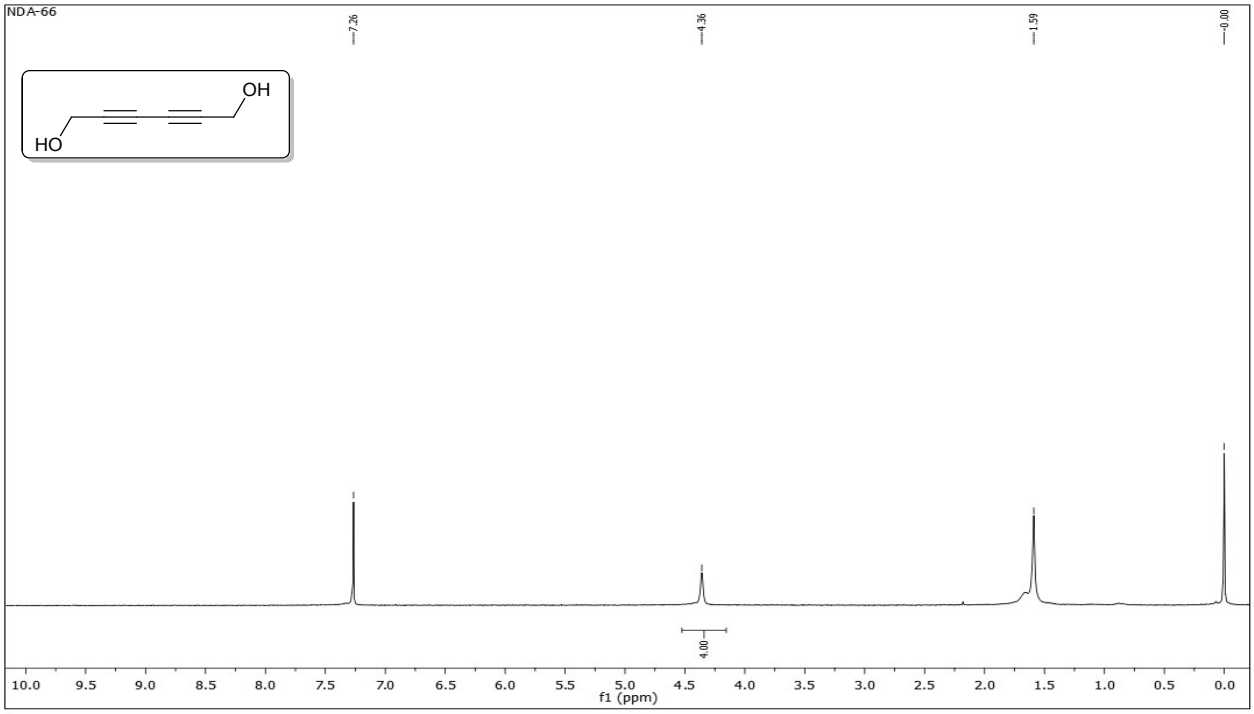

Fig. S49 ^{1}H NMR spectrum of Hexa-2,4-diyne-1,6-diol **(3p)** (300 MHz, $CDCl_3$)

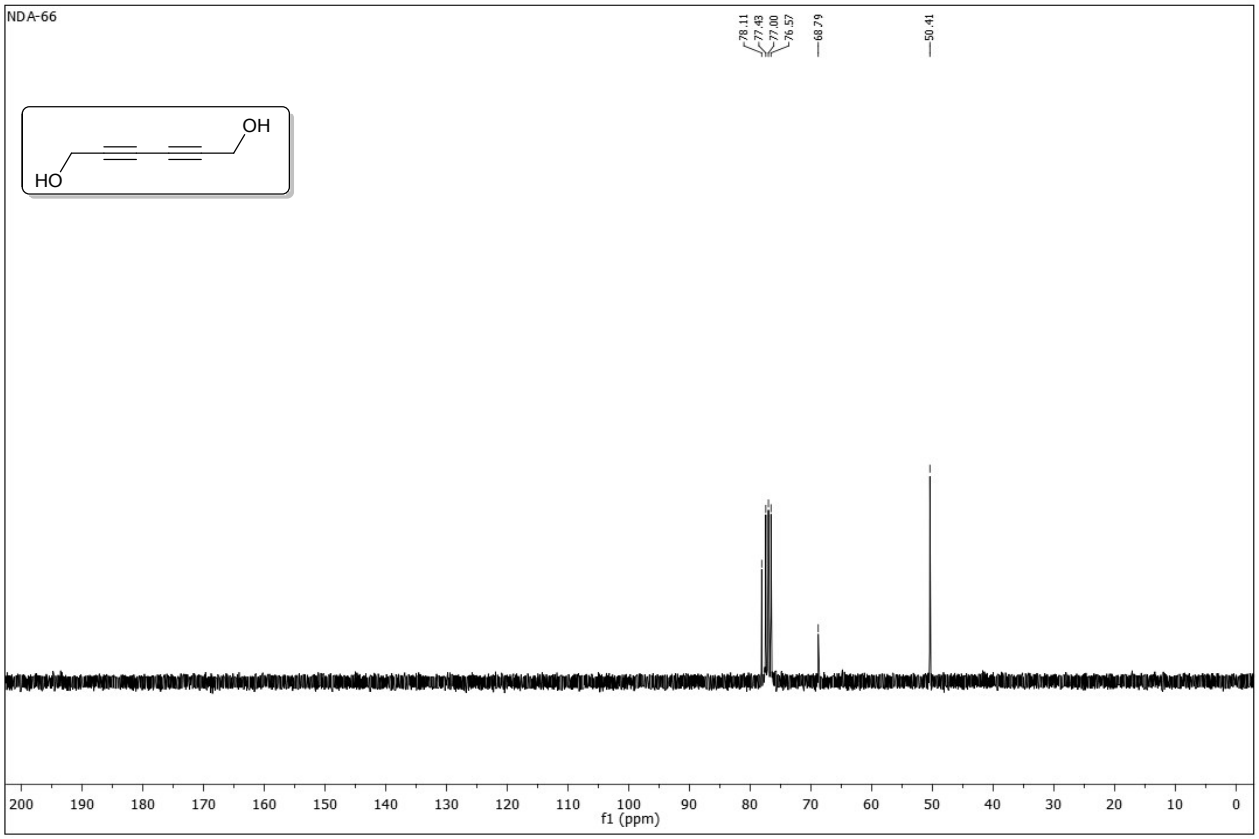

Fig. S50 ^{1}H NMR spectrum of Hexa-2,4-diyne-1,6-diol **(3p)** (75 MHz, $CDCl_3$)

6. EI-MS Spectra of isolated Compounds from 3a – 3p:

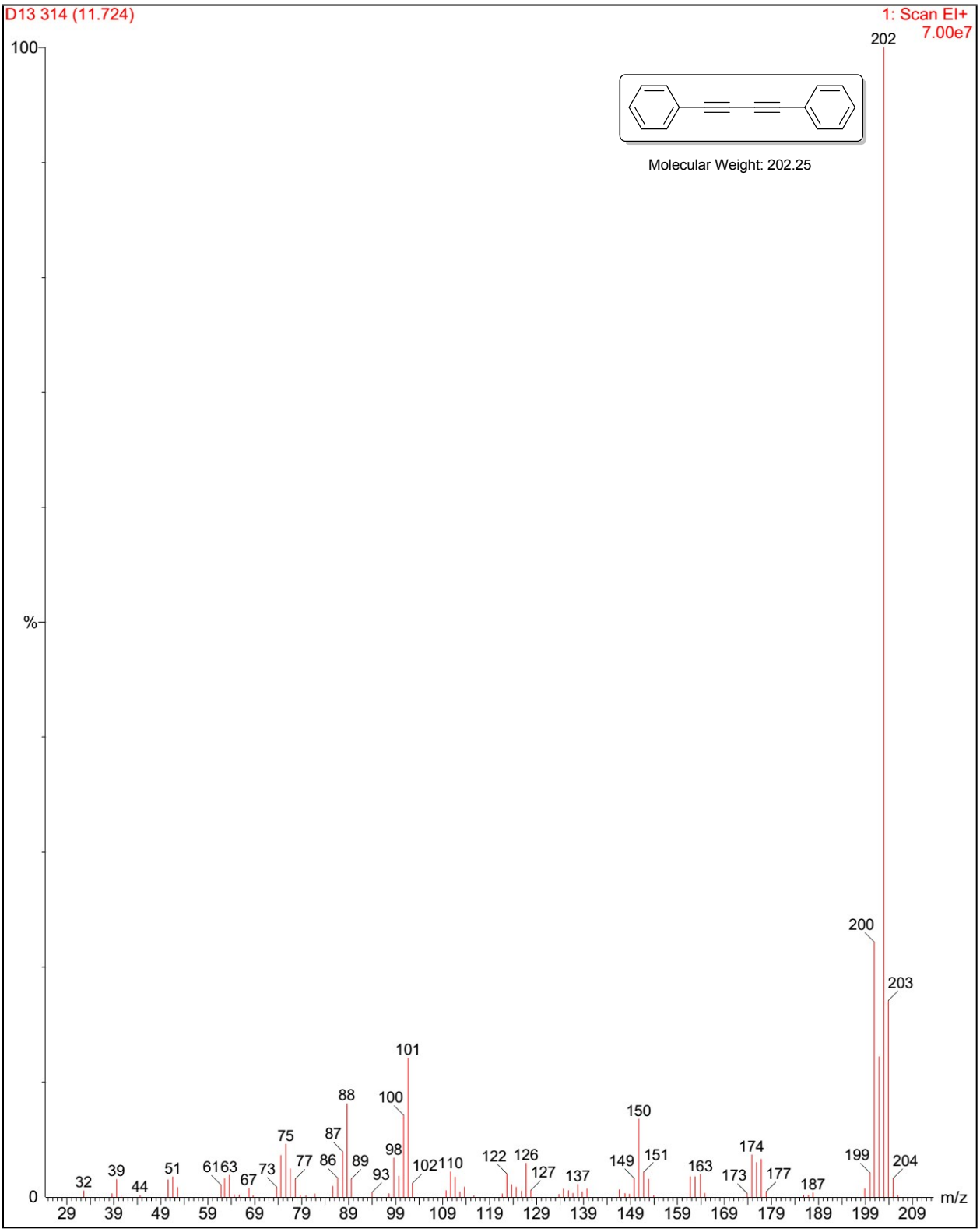

Fig. S51 EI-MS for 1,4-diphenylbuta-1,3-diyne **(3a)**

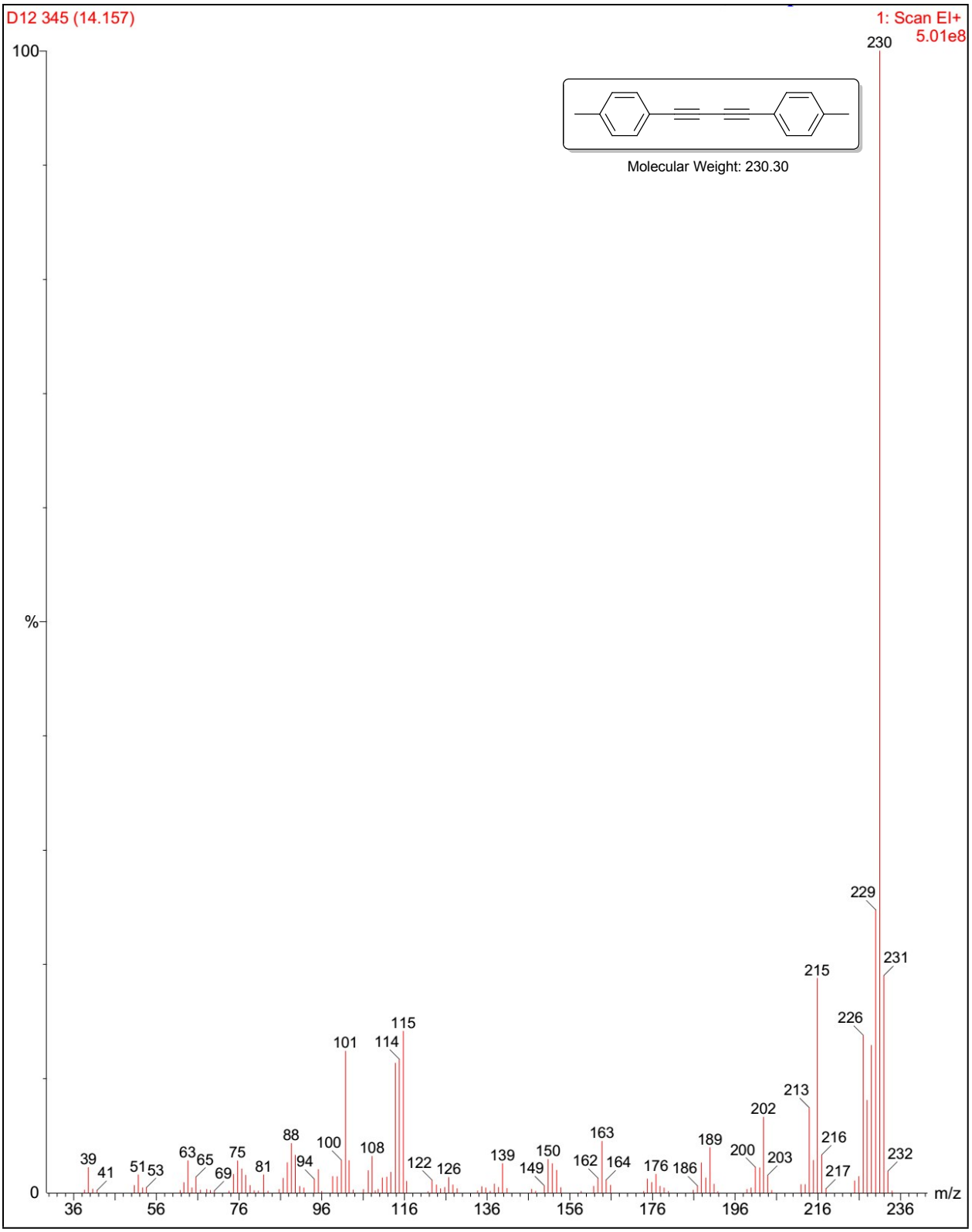

Fig. S52 EI-MS for 1,4-di-*p*-tolylbuta-1,3-diyne **(3b)**

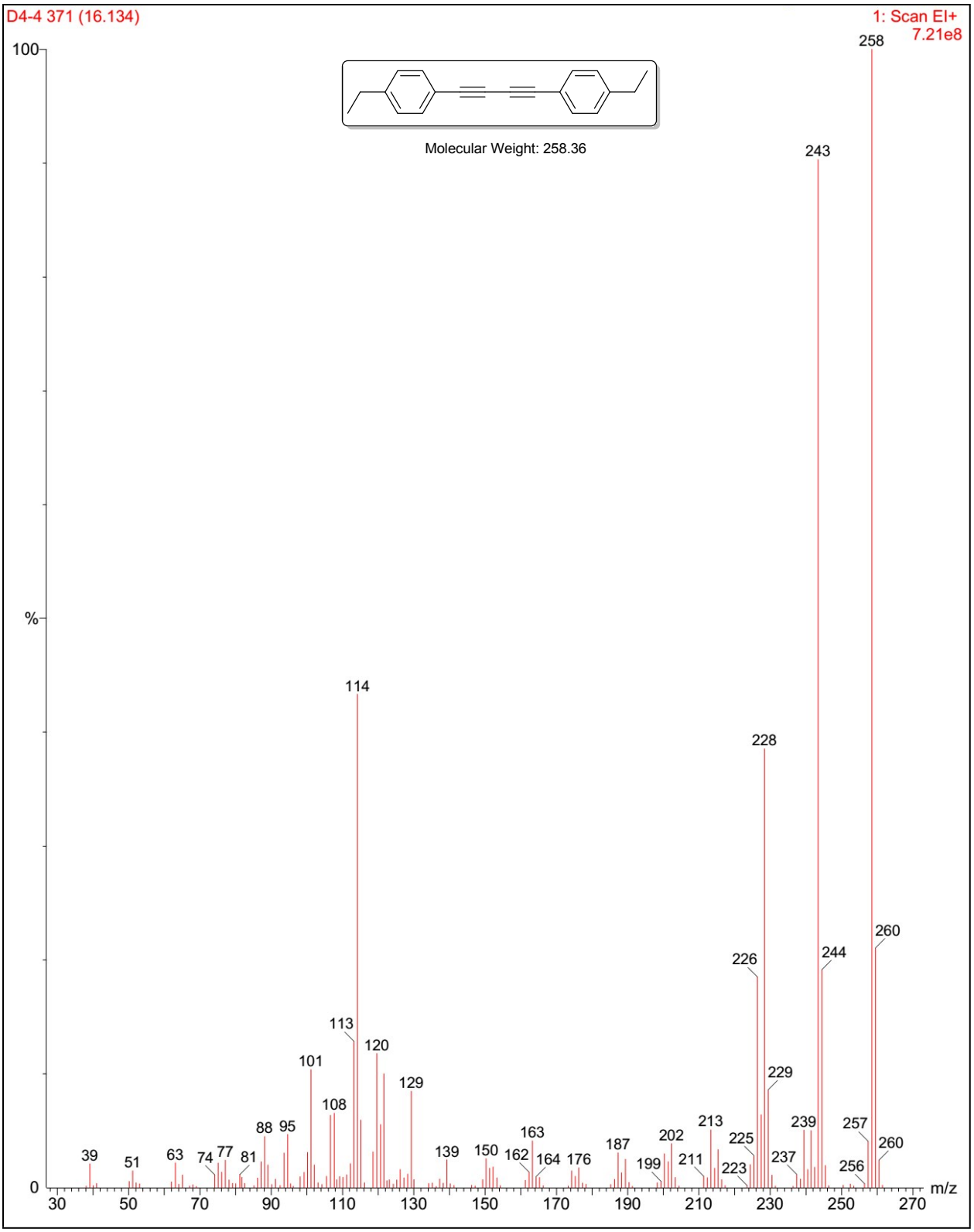

Fig. S53 EI-MS for 1,4-bis(4-ethylphenyl)buta-1,3-diyne **(3c)**

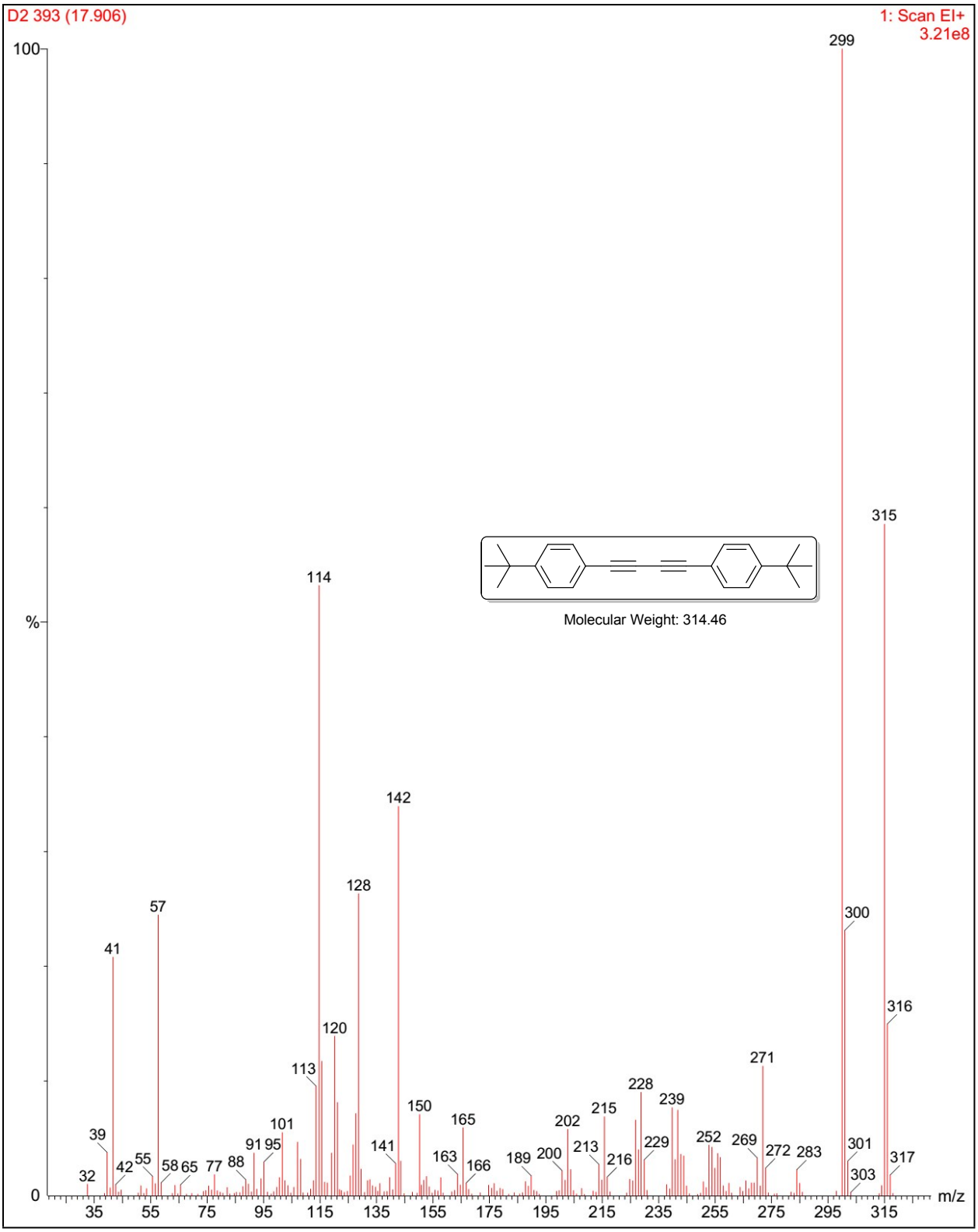

Fig. S54 EI-MS for 1,4-bis(4-(*tert*-butyl)phenyl)buta-1,3-diyne **(3d)**

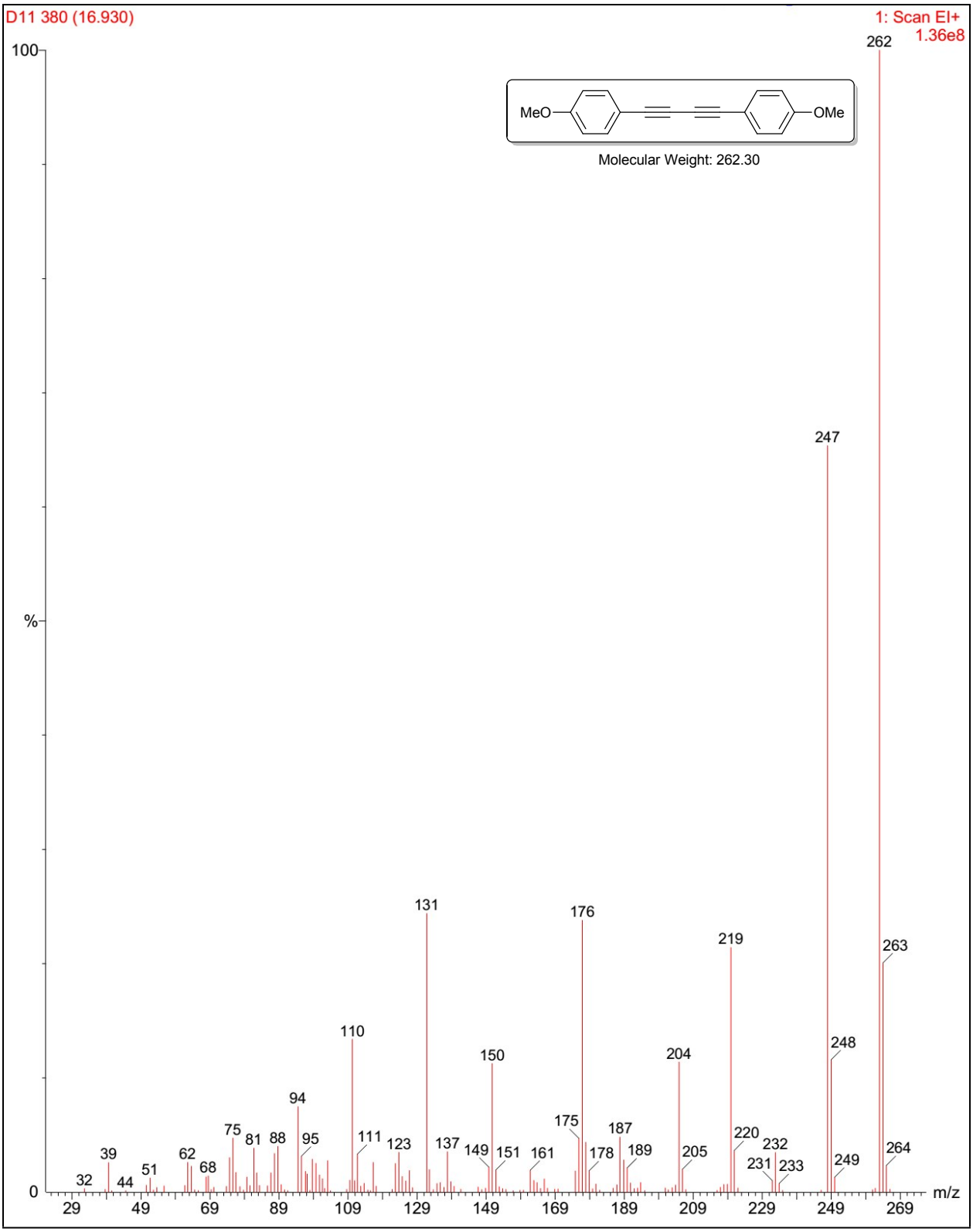

Fig. S55 EI-MS for 1,4-bis(4-methoxyphenyl)buta-1,3-diyne **(3e)**

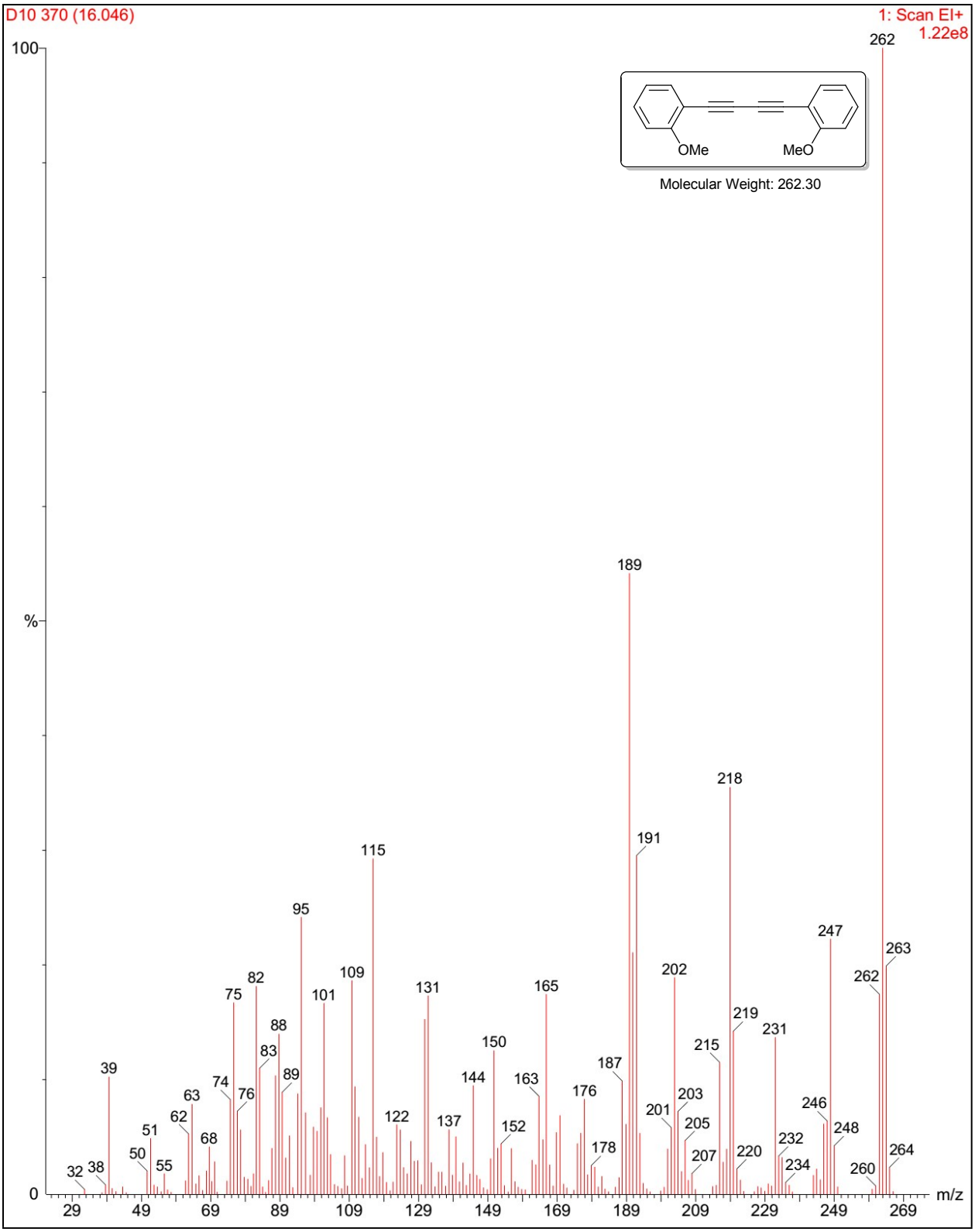

Fig. S56 EI-MS for 1,4-bis(2-methoxyphenyl)buta-1,3-diyne **(3f)**

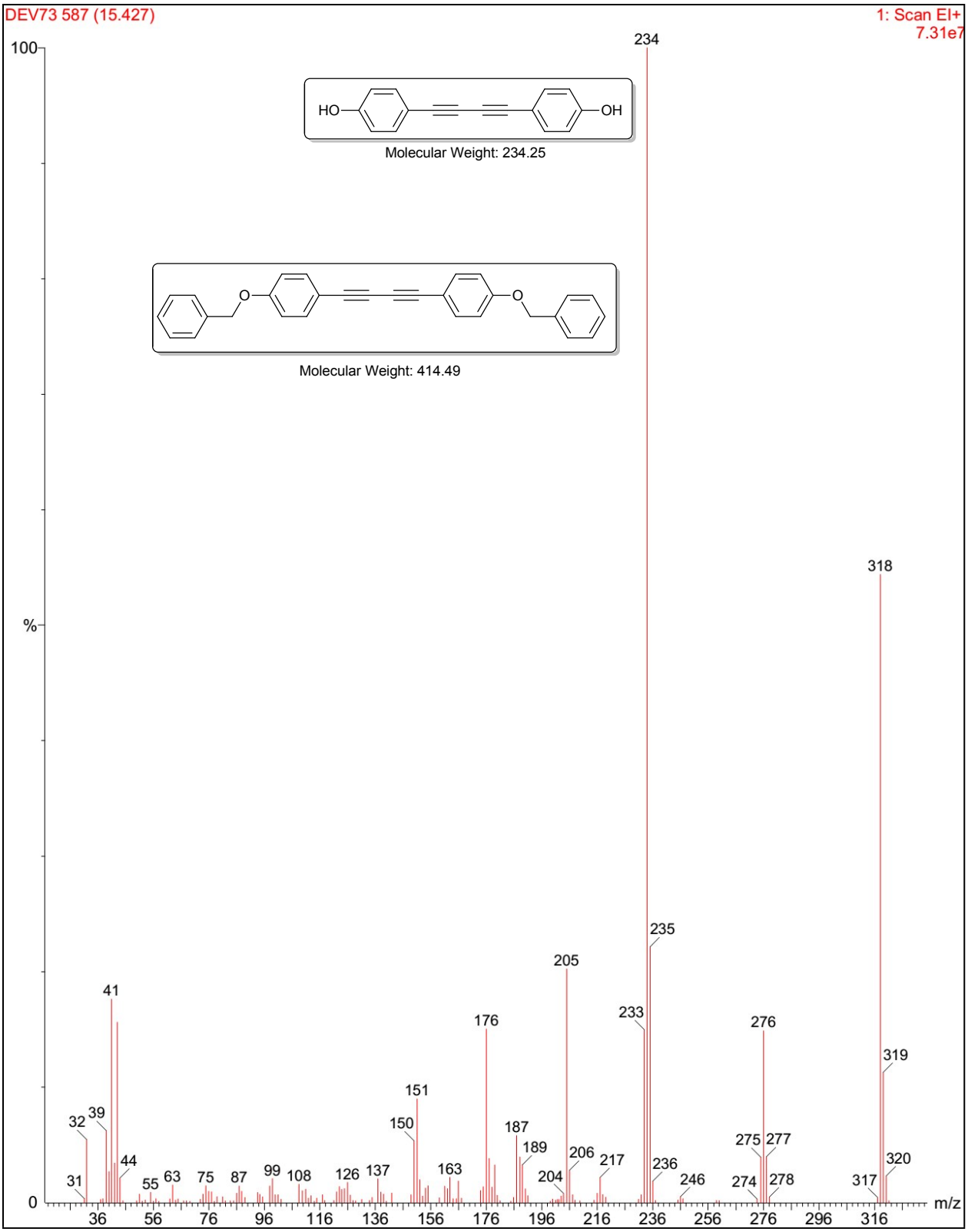

Fig. S57 EI-MS for 1,4-bis(4-(benzyloxy)phenyl)buta-1,3-diyne **(3h)**

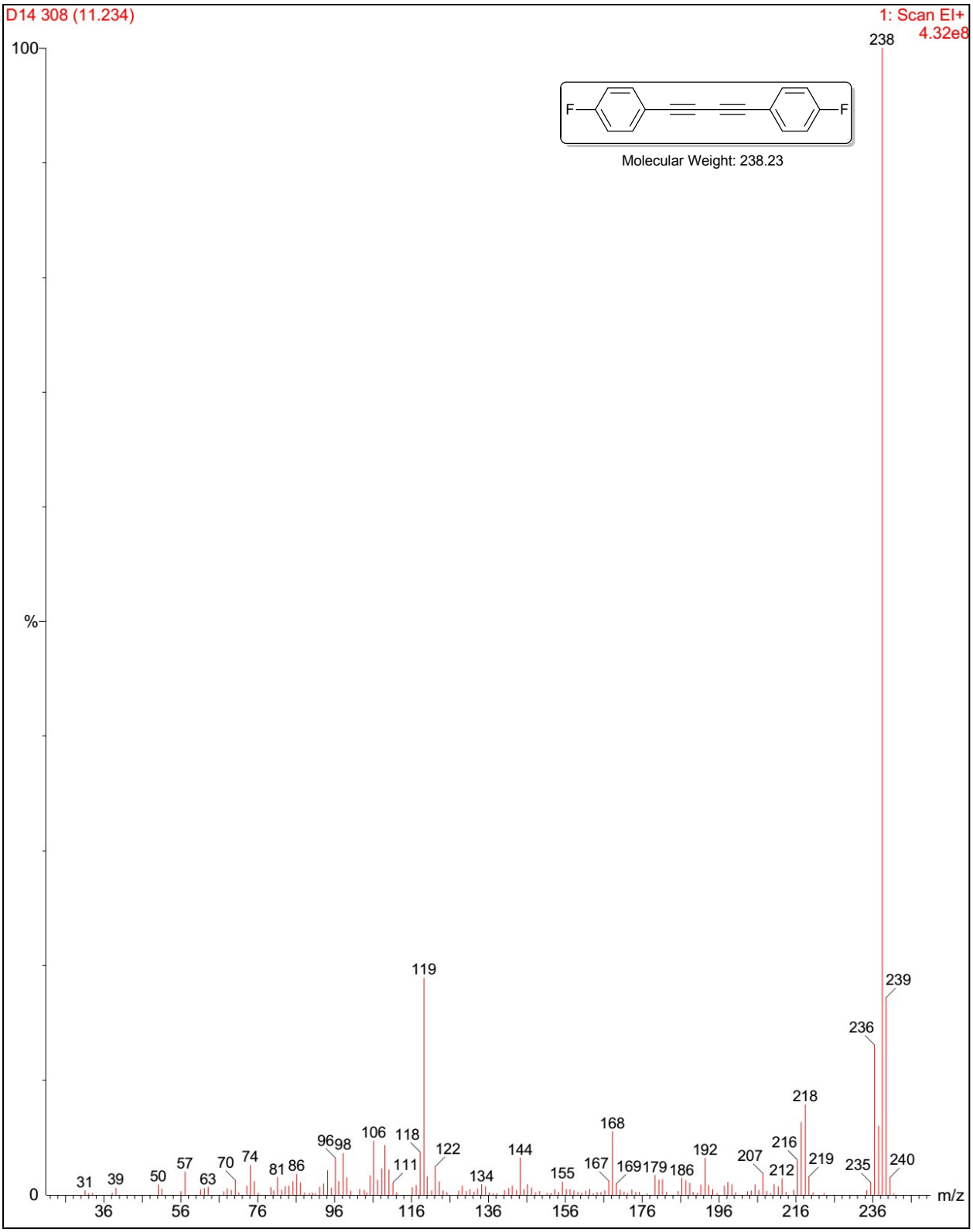

Fig. S58 EI-MS for 1,4-bis(4-fluorophenyl)buta-1,3-diyne **(3i)**

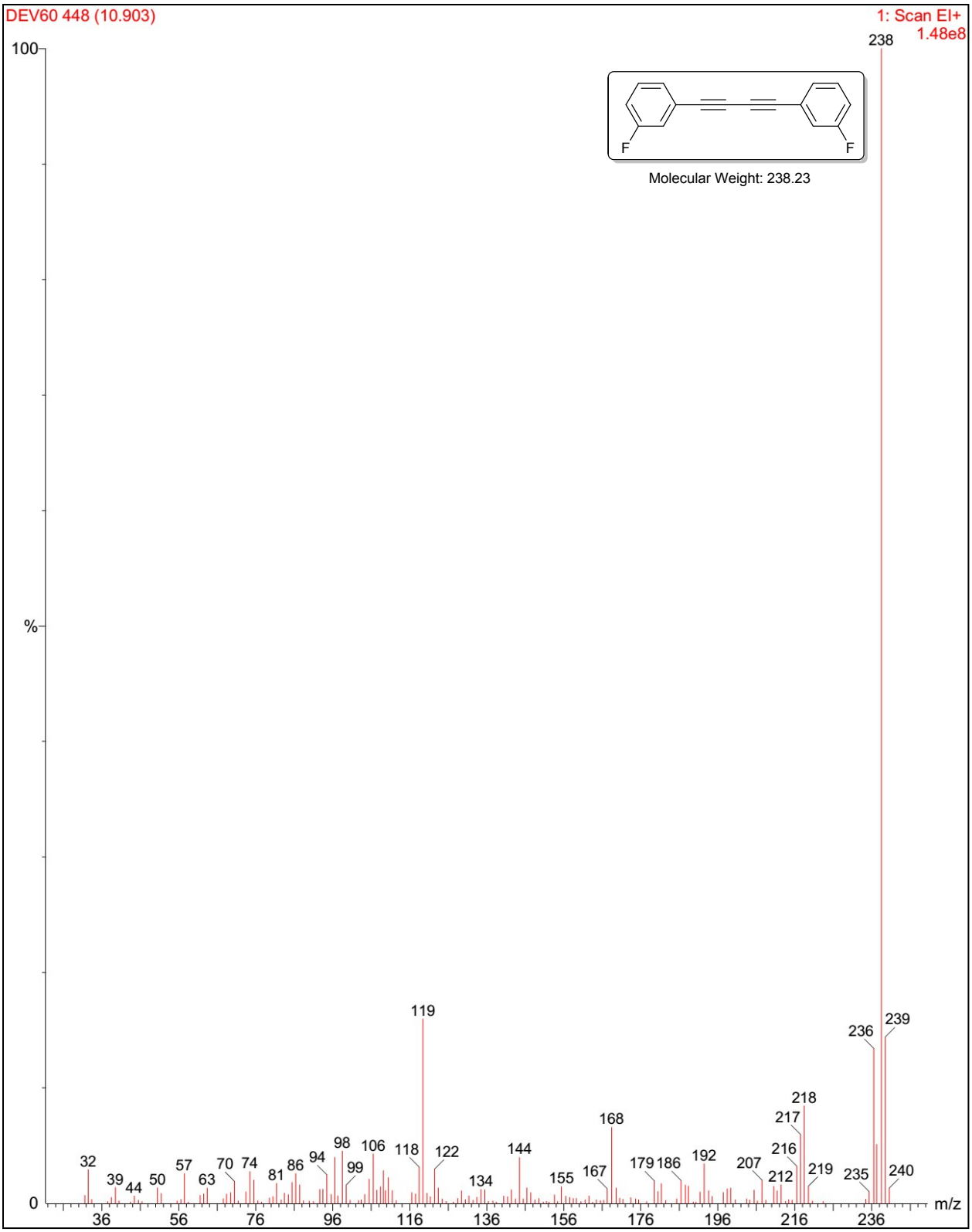

Fig. S59 EI-MS for 1,4-bis(3-fluorophenyl)buta-1,3-diyne **(3j)**

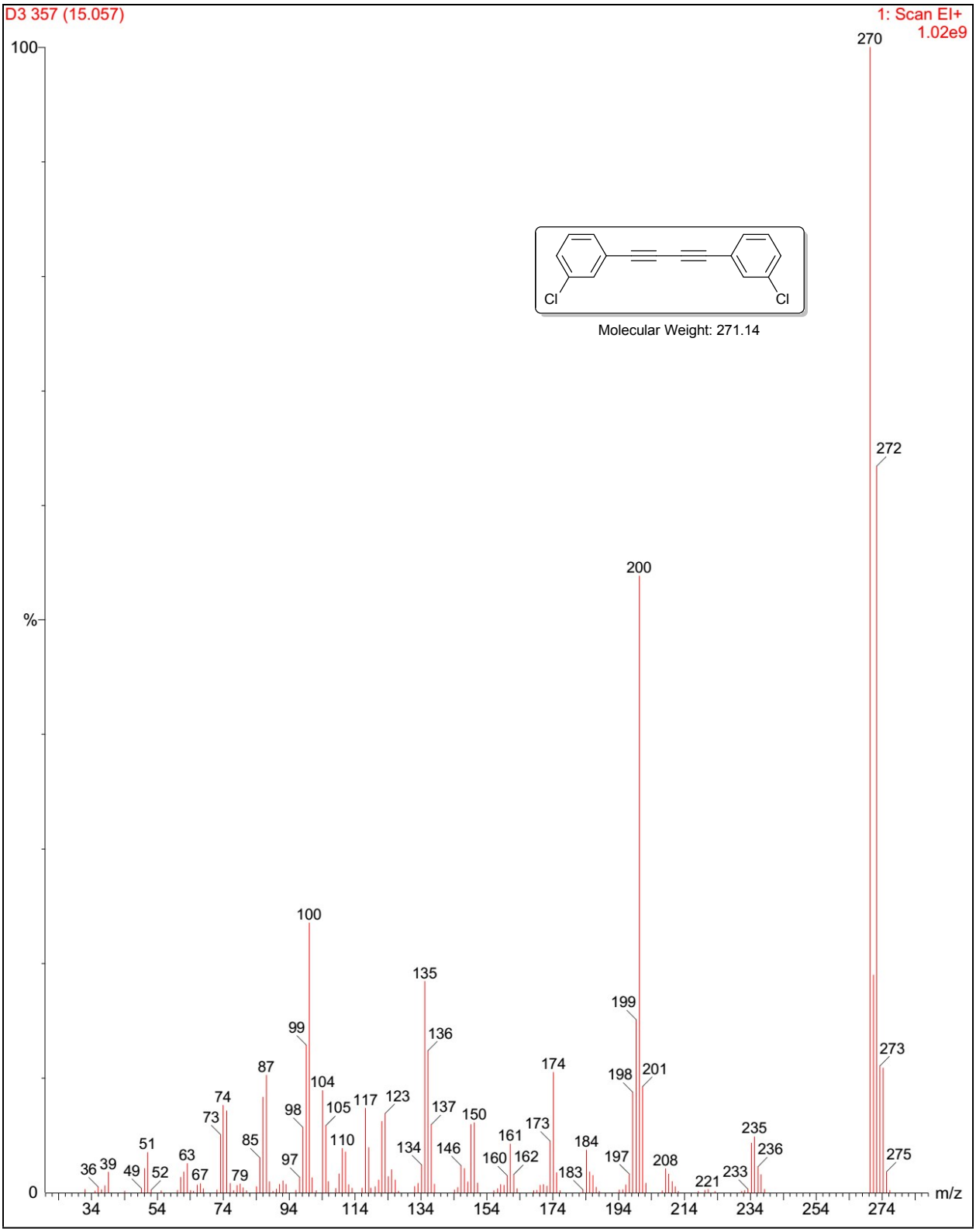

Fig. S60 EI-MS for 1,4-bis(3-chlorophenyl)buta-1,3-diyne **(3k)**

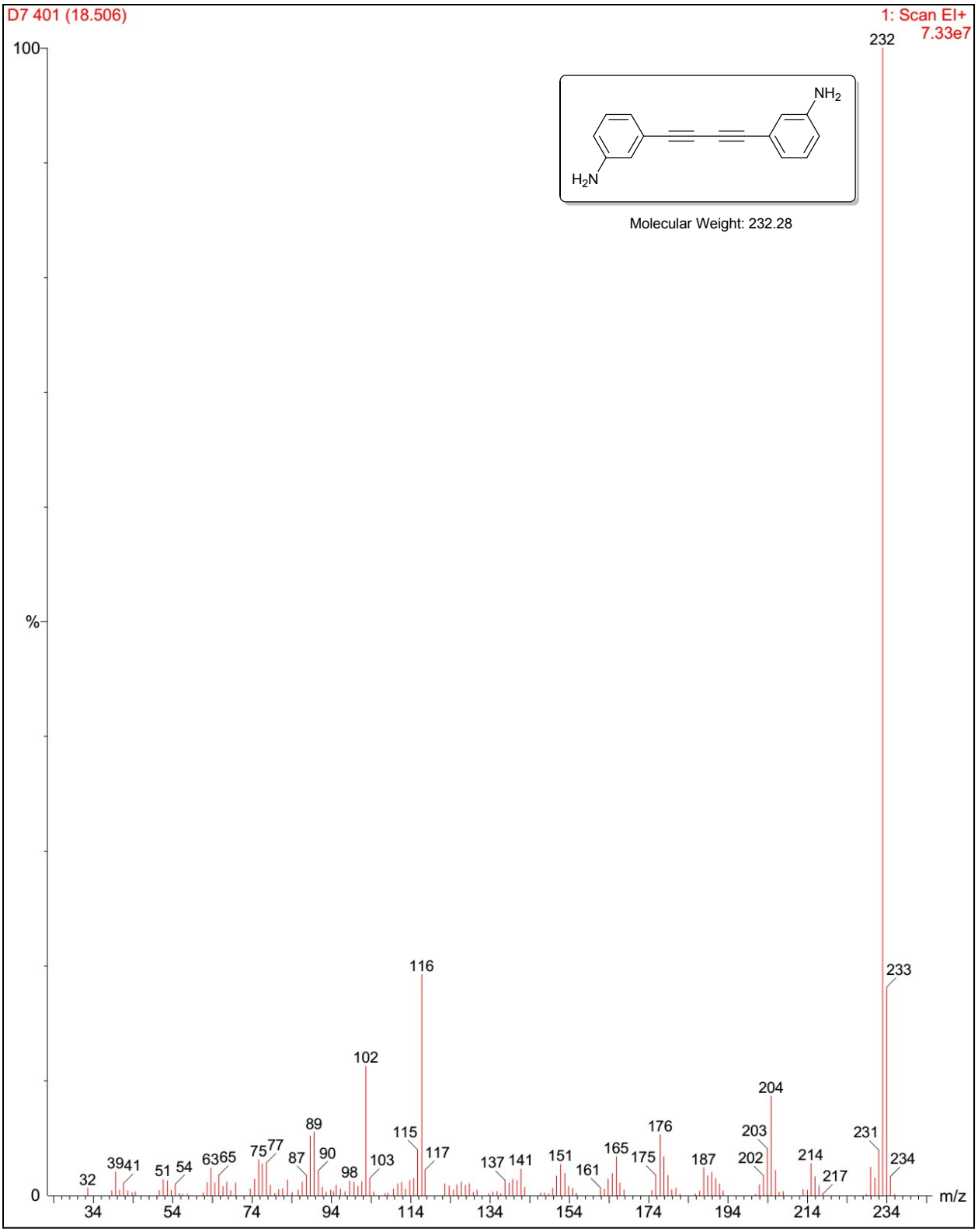

Fig. S61 EI-MS for 3,3'-(buta-1,3-diyne-1,4-diyl)dianiline **(3l)**

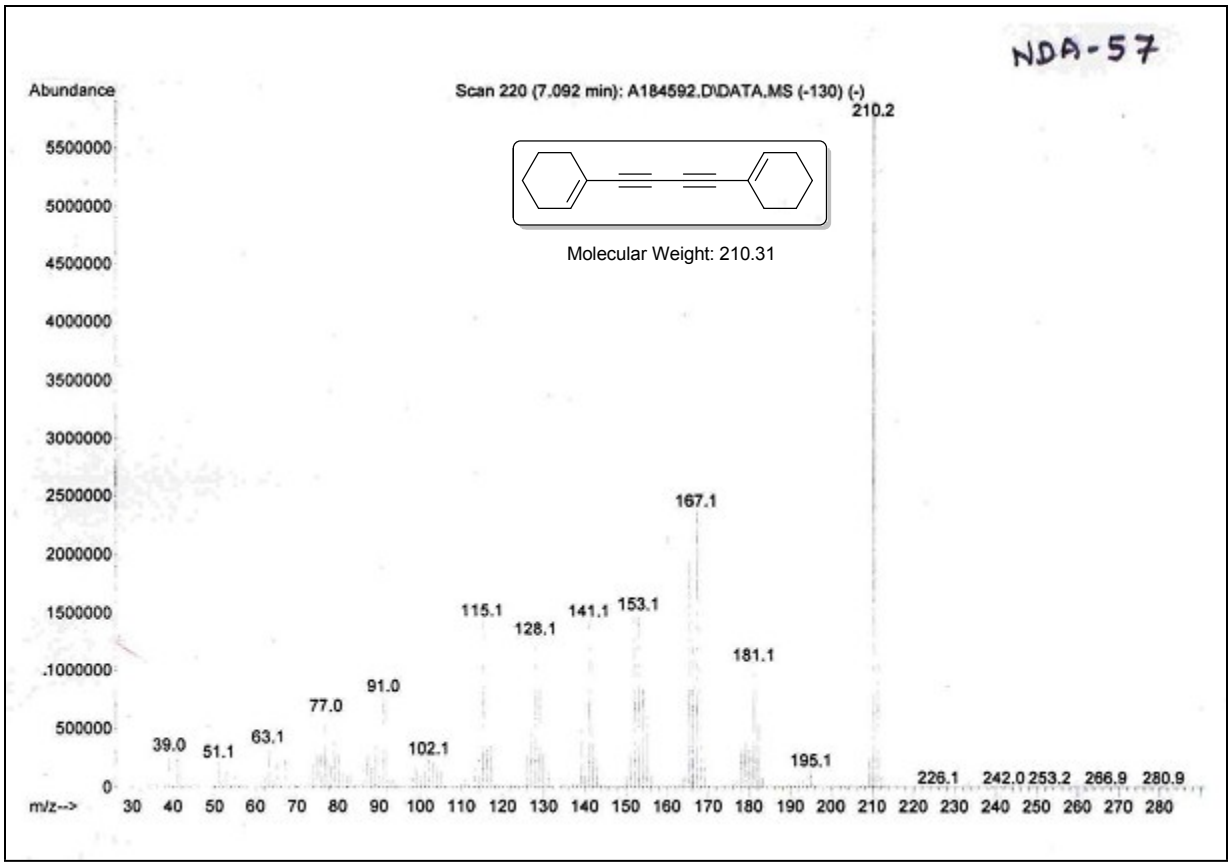

Fig. S62 EI-MS for 1,4-di(cyclohex-1-en-1-yl)buta-1,3-diyne **(3m)**

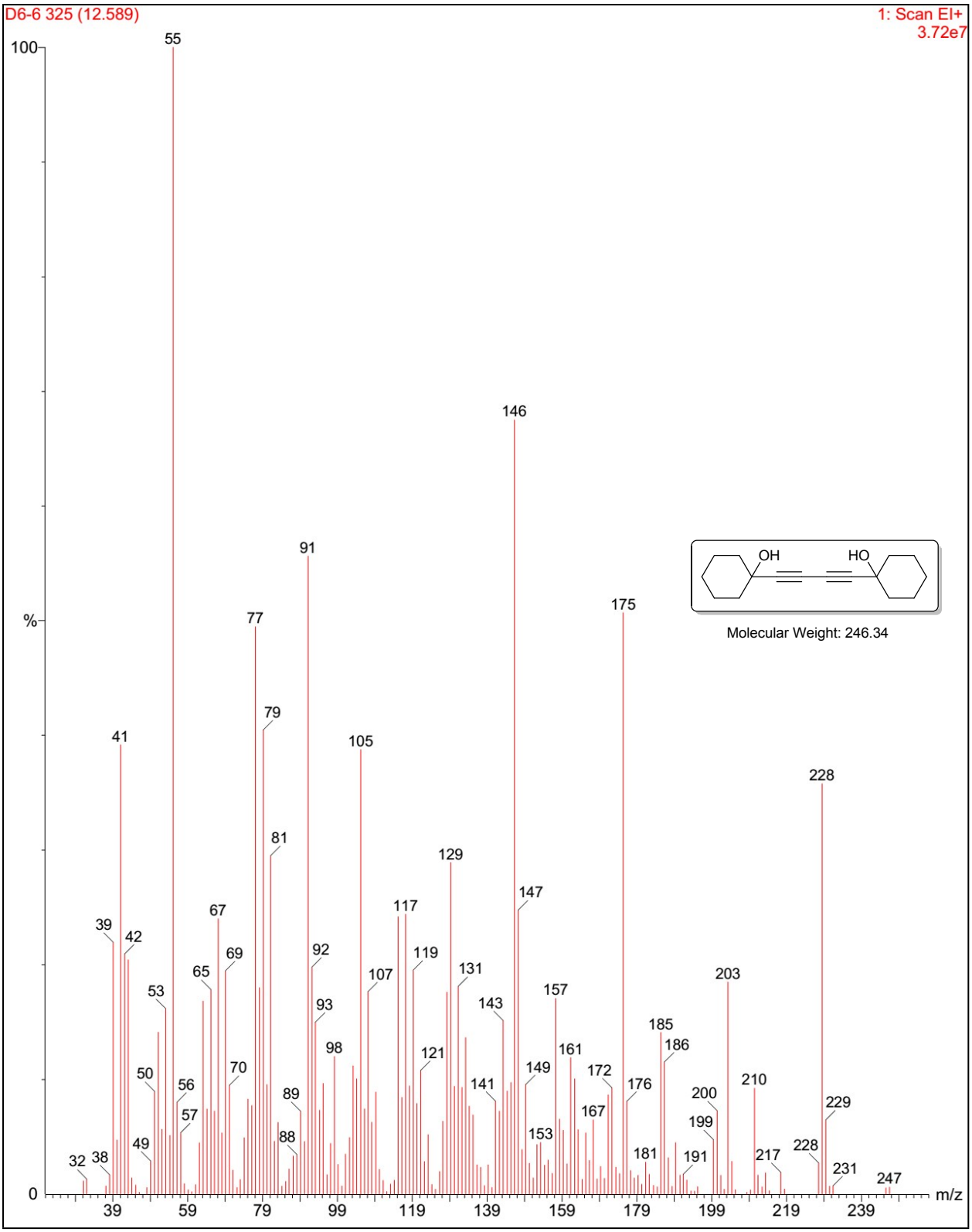

Fig. S63 EI-MS for 1,1'-(buta-1,3-diyne-1,4-diyl)dicyclohexanol **(3n)**

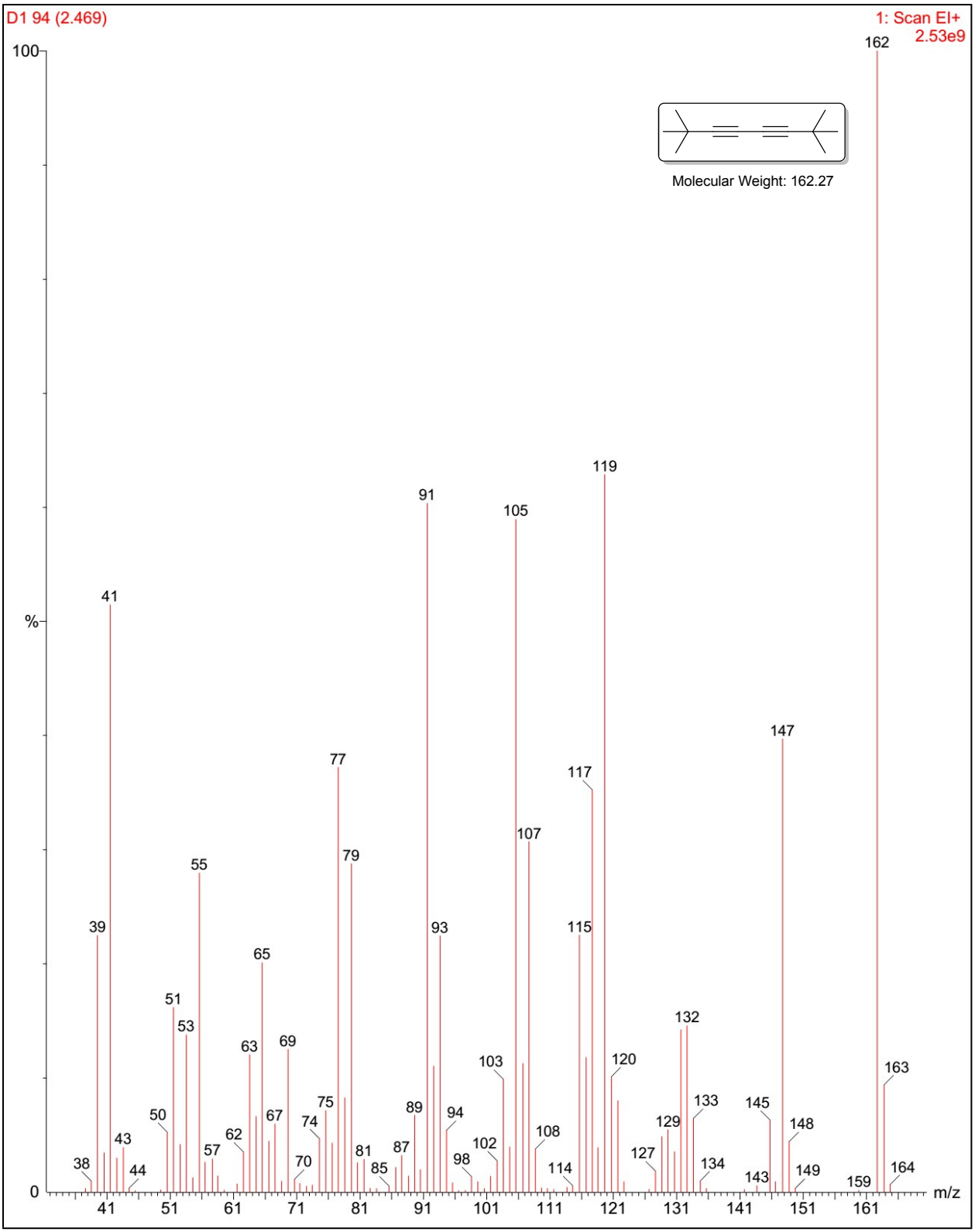

Fig. S64 EI-MS for 2,2,7,7-tetramethylocta-3,5-diyne **(3o)**

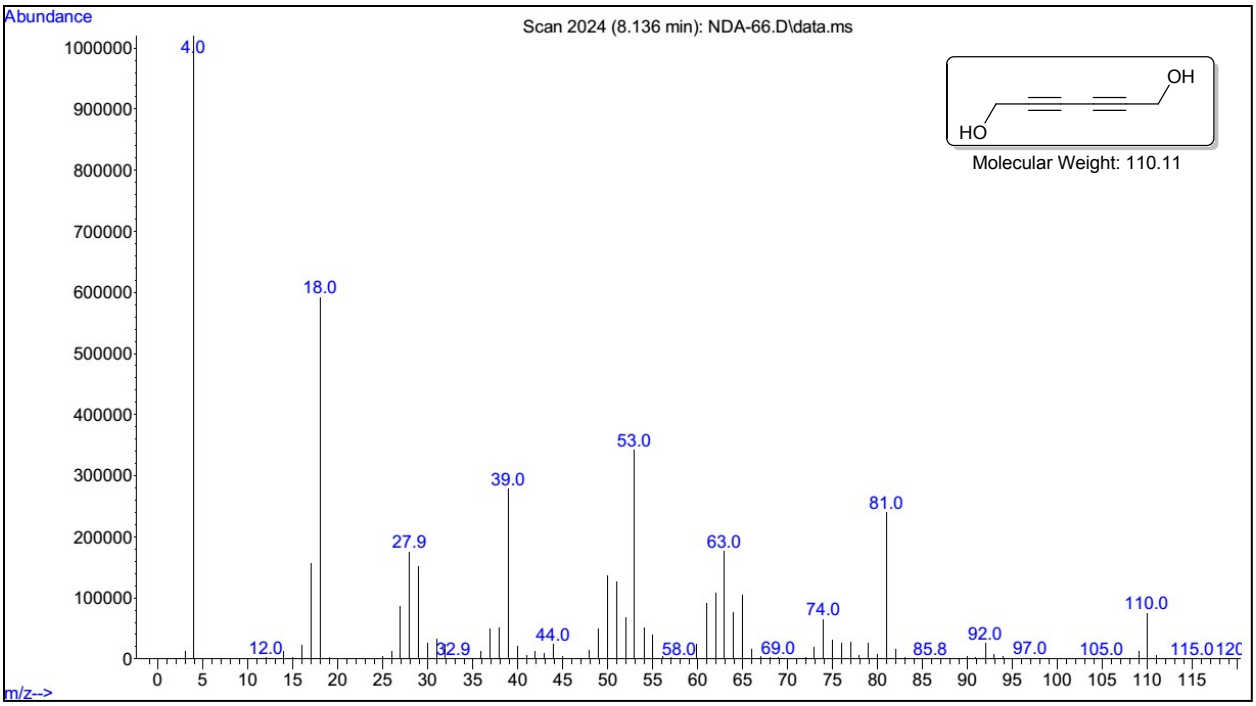

Fig. S65 EI-MS for Hexa-2,4-diyne-1,6-diol **(3p)**